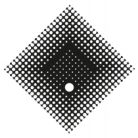
VICTORIA UNIVERSITY
MELBOURNE AUSTRALIA

Multi-Criteria Analysis of a Developed Prefabricated Footing System on Reactive Soil Foundation

This is the Published version of the following publication

Teodosio, Bertrand, Bonacci, Francesco, Seo, Seongwon, Baduge, Kasun Shanaka Kristombu and Mendis, Priyan (2021) Multi-Criteria Analysis of a Developed Prefabricated Footing System on Reactive Soil Foundation. Energies, 14 (22). p. 7515. ISSN 1996-1073

The publisher's official version can be found at
https://www.mdpi.com/1996-1073/14/22/7515
Note that access to this version may require subscription.

Downloaded from VU Research Repository https://vuir.vu.edu.au/42826/

energies

MDPI

Article

Multi-Criteria Analysis of a Developed Prefabricated Footing System on Reactive Soil Foundation

Bertrand Teodosio [1,*], Francesco Bonacci [2], Seongwon Seo [3], Kasun Shanaka Kristombu Baduge [3] and Priyan Mendis [3]

[1] Institute of Sustainable Industries and Liveable Cities, Victoria University, Melbourne 3011, Australia
[2] Cardno, Melbourne 3000, Australia; francesco.bonacci@cardno.com.au
[3] Department of Infrastructure Engineering, The University of Melbourne, Parkville 3010, Australia; seongwon.seo@unimelb.edu.au (S.S.); kasun.kristombu@unimelb.edu.au (K.S.K.B.); pamendis@unimelb.edu.au (P.M.)
* Correspondence: bertrand.teodosio@vu.edu.au; Tel.: +61-410-517-555

Abstract: The need for advancements in residential construction and the hazard induced by the shrink–swell reactive soil movement prompted the development of the prefabricated footing system of this study, which was assessed and compared to a conventional waffle raft using a multi-criteria analysis. The assessment evaluates the structural performance, cost efficiency, and sustainability using finite element modelling, life cycle cost analysis, and life cycle assessment, respectively. The structural performance of the developed prefabricated system was found to have reduced the deformation and cracking by approximately 40%. However, the cost, GHG emission, and embodied energy were higher in the prefabricated footing system due to the greater required amount of concrete and steel than that of the waffle raft. The cost difference between the two systems can be reduced to as low as 6% when prefabricated systems were installed in a highly reactive sites with large floor areas. The life cycle assessment further observed that the prefabricated footing systems consume up to 21% more energy and up to 18% more GHG emissions. These can significantly be compensated by reusing the developed prefabricated footing system, decreasing the GHG emission and energy consumption by 75–77% and 55–59% with respect to that of the waffle raft.

Keywords: prefabricated footing system; reactive soil foundation; finite element model (FEM); life cycle assessment (LCA); green house gases (GHG); life cycle cost (LCC)

check for updates

Citation: Teodosio, B.; Bonacci, F.; Seo, S.; Baduge, K.S.K.; Mendis, P. Multi-Criteria Analysis of a Developed Prefabricated Footing System on Reactive Soil Foundation. *Energies* **2021**, *14*, 7515. https://doi.org/10.3390/en14227515

Academic Editor: Umberto Desideri

Received: 24 September 2021
Accepted: 8 November 2021
Published: 10 November 2021

Publisher's Note: MDPI stays neutral with regard to jurisdictional claims in published maps and institutional affiliations.

Copyright: © 2021 by the authors. Licensee MDPI, Basel, Switzerland. This article is an open access article distributed under the terms and conditions of the Creative Commons Attribution (CC BY) license (https://creativecommons.org/licenses/by/4.0/).

1. Introduction

Prefabricated construction refers to the process of building a structure through off-site manufacturing of elements under controlled conditions and then transporting and assembling it on-site. This can potentially alleviate the challenges experienced by the Architecture, Engineering and Construction (AEC) industry since prefabrication expedites the total construction period by eliminating delays due to weather impact and skilled labour shortages [1–5]. Prefabricated construction is also a more sustainable option for reducing the generation of waste considering the entire life cycle stages of a building, and further enables a reusable and relocatable structure [6–8]. Furthermore, prefabricated systems have better and more consistent quality through a controlled manufacturing process and a safer working environment [9–11].

Most observed prefabrication advancements have been focusing on superstructures, while the conventional cast-in-situ method, particularly for concrete structures, is still the preferred construction technique for footing systems [12]. The full potential of prefabricated construction is yet to be fully realised since most innovations have been focusing on the superstructures of buildings.

Prefabrication of footing systems requires an inter-disciplinary approach to consider critical manufacturing, structural and geotechnical aspects [13]. Important considerations

include the appropriate design to account for the susceptibility of the footings of lightweight structures on clayey footings to severe damage induced by reactive soils [14,15]. Reactive soils are clayey footings, which undergo a significant change in volume due to seasonal soil water content changes. These soils experience swelling when the water level increases and shrinking when the water level decreases [16,17]. The difference in soil water level between the uncovered ground, where evaporation, transpiration and precipitation take place, and the covered ground, where impermeable footings are constructed, causes differential ground movement (Figure 1). The shrink–swell soil movement causes structural deformation through soil–structure interaction. This is crucial for lightweight structures such as houses, garages and pavements [18,19]. Repair cost amounts to billions of dollars worldwide to mitigate the damage induced by the shrinking and swelling of reactive soils [13,20–23].

Due to the absence of prefabricated footing systems for houses, a prefabricated design was developed considering the detrimental effects inflicted by the shrink–swell ground movement. The main aim of this study is to present and assess the global structural performance, cost efficiency, and sustainability of a developed prefabricated footing system using a multi-criteria analysis. The multi-criteria analysis will be based on structural performance, life cycle cost (LCC) analysis, and life cycle assessment (LCA). The developed prefabricated footing system is compared to a conventional in-situ monolithic waffle raft.

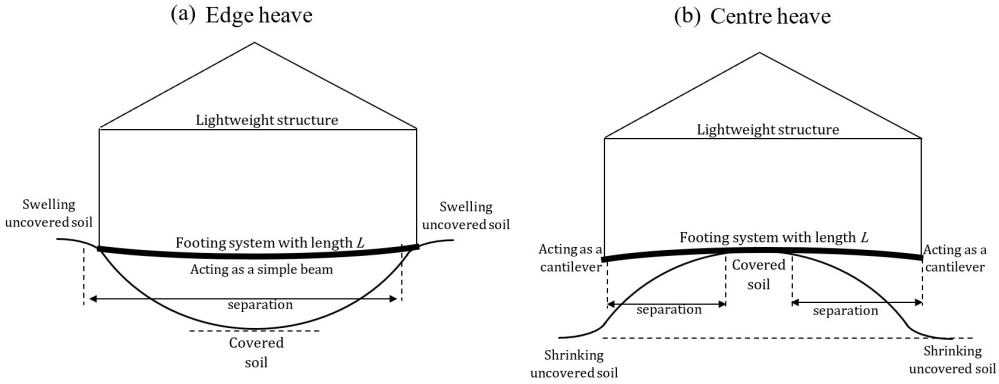

Figure 1. Two cases of reactive soil heaving: (**a**) edge heaving due to the swelling uncovered ground, and (**b**) centre heaving due to the shrinking uncovered ground.

2. Methodology

The developed prefabricated footing system is assessed and compared to a conventional in-situ monolithic waffle raft. The comparison will determine which option has a more sustainable design based on three criteria, as described in Figure 2a, having better structural performance, more cost efficient, and lesser environmental impact. The developed prefabricated footing system is presented in the following section, whilst the design of the conventional waffle rafts followed the design stipulations in AS 2870-2011 by [24]. The multi-criteria analysis will evaluate the structural performance using a coupled hydro-mechanical FEM, cost analysis using LCC, and environmental impact (GHG and embodied energy) using LCA, as described in Figure 2b and discussed in the following sections.

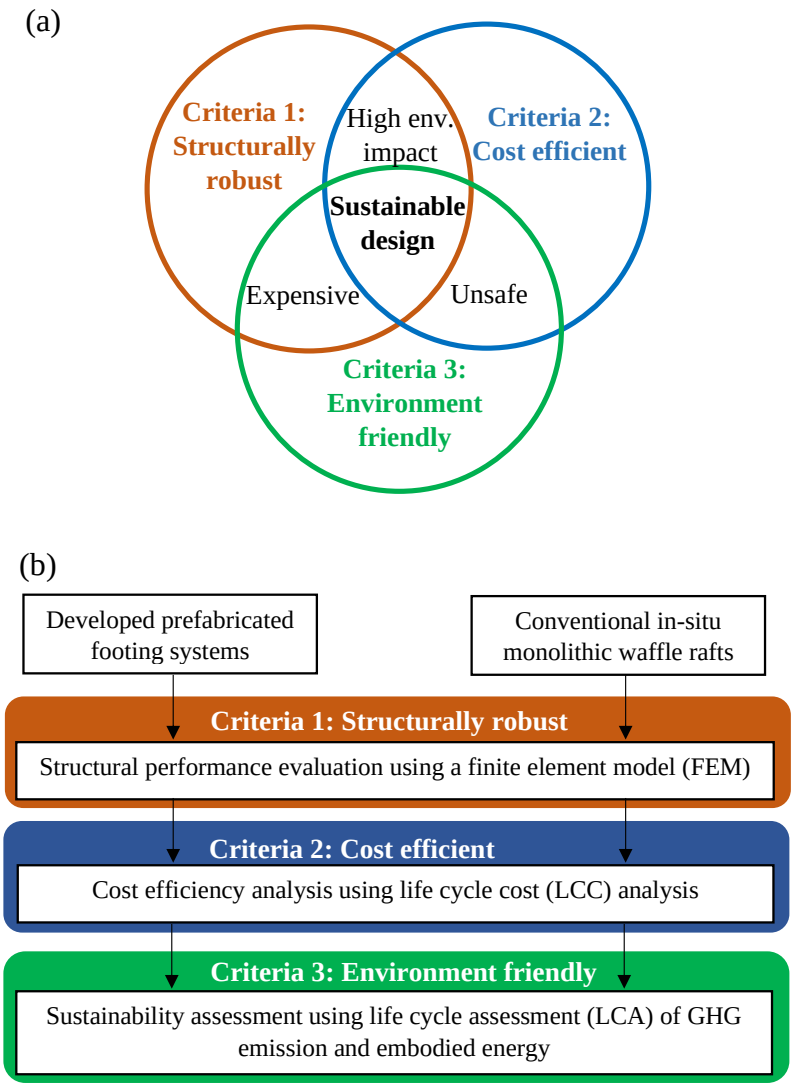

Figure 2. Methodology of the study: (**a**) the concept of the multi-criteria analysis to achieve a sustainable design and (**b**) the multi-criteria comparison between the developed prefabricated footing systems and the conventional in-situ monolithic waffle rafts.

2.1. The Developed Prefabricated Footing

The developed prefabricated footing system had a constant floor area of 225 m^2 (15 by 15 m^2), since the average floor area of single-detached dwellings in Australia is approximately 230 m^2 [18].

Dimensional coordination is considered in the design of the developed prefabricated footing system. This manufacturing concept organises different elements independently with the goal of being connected and integrated as a whole system [25,26]. This approach does improve the assembly of a structure considering strict tolerance and improves the design flexibility of structural components. The hypothetical developed prefabricated footing systems with a 225 m^2-floor area are divided into three main components to achieve dimensional coordination. The three main components are: (1) the developed dapped-end beams (DEB) and bolt connection; (2) connectors (i.e., 2-way, 3-way and 4-way connectors); and (3) slabs. The plan view of the developed prefabricated footing systems showing the three main components is presented in Figure 3. These structural elements were also designed considering the dimensional limits for handling and transportation. Through the connectors, the length of the DEB can be varied depending on the required span of the entire footing floor area achieving dimensional coordination.

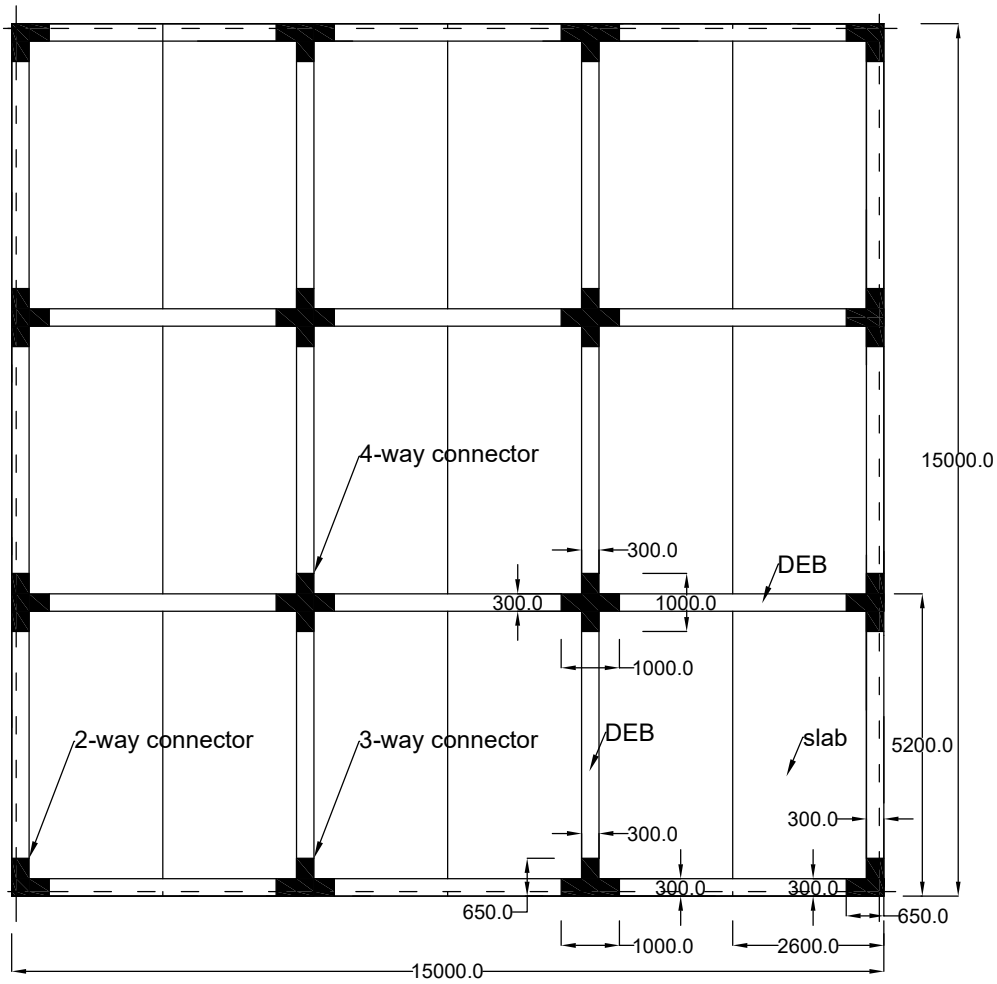

Figure 3. Plan view of the developed prefabricated footing systems (length in mm).

Sites in Australia are classified based on the reactivity of founding soils where structures are being constructed described in Standards Australia [24]. The reactivity of soil is related to the characteristic surface movement, y_s, presented in Table 1, calculated as:

$$y_s = \frac{1}{100}\sum_{n=1}^{N}(I_{pt}\Delta\overline{u}h_{soil})_n = \frac{1}{100}\sum_{n=1}^{N}(\alpha I_{ss}\Delta\overline{u}h_{soil})_n, \quad (1)$$

where I_{pt} is the index for instability (in pF), $\Delta\overline{u}$ is the average change in soil suction over the thickness of the soil layer being considered (in pF), α is a factor to consider soil lateral restraint, I_{ss} is an index for soil shrinkage (in %/pF), h_{soil} is the thickness of the soil layer being considered (in m), and N is the assumed number of soil layers. The specified design of footing systems, in this specific case the hypothetical waffle rafts, will be dependent on the site classification outlining the required beam dimensions and steel reinforcements.

Performance of the prefabricated footing design for each site classification in Table 1 was compared to waffle rafts as stipulated in AS 2870.4.6 [24]. The values of unit stiffness (EI/L) of the monolithic waffle rafts required for each site class were first calculated using Standards Australia [24]:

$$\frac{EI}{L} = log\left[\frac{\sum\frac{B_w D^3}{12}}{W}\right], \quad (2)$$

where B_w is the width of the external and internal beams (in mm), D is the depth of beams (in mm), and W is the width of a slab perpendicular to L (in m). The hypothetical waffle rafts had a constant slab thickness of 85 mm. Steel reinforcements were 3–16 mm

⌀ (3N16) for the edge beams, 1–16 mm ⌀ (1N16) for the internal beams, and 8 mm ⌀ spaced at 200 mm (SL82) for the slab mesh, as stipulated in Standards Australia [24]. Using Equation (2), EI/L for each site classification was calculated and was used to determine the equivalent dimensions of the hypothetical prefabricated footing systems per site class. This will effectively compare the structural performance between the hypothetical monolithic waffle rafts and the developed prefabricated footing systems for each site class (i.e., Class M/M-D, Class H_1/H_1-D and H_2/Class H_2-D). The calculated EI/L and the corresponding concrete beam dimensions are shown in Table 2. The section of the developed prefabricated footing system for each site class is described in Figure 4.

Table 1. Classification of site based on reactivity of soil and soil movement, y_s, as described in the Australian Standard (AS) 2870-2011 [24].

Class	Soil Footing	y_s (mm)
A	gravelly and sandy soil	0
S	slightly reactive silt or clay soil	0 to 20
M	moderately reactive silt or clay soil	20 to 40
H_1	highly reactive clay soil	40 to 60
H_2	very highly reactive clay soil	60 to 75
E	extremely reactive clay soil	greater than 75
P	filled, soft silt or clay, loose sands, sandslip, mine subsidence, collapsing	varying
D	areas having deep-seated soil moisture changes shall use a suffix "-D"	-

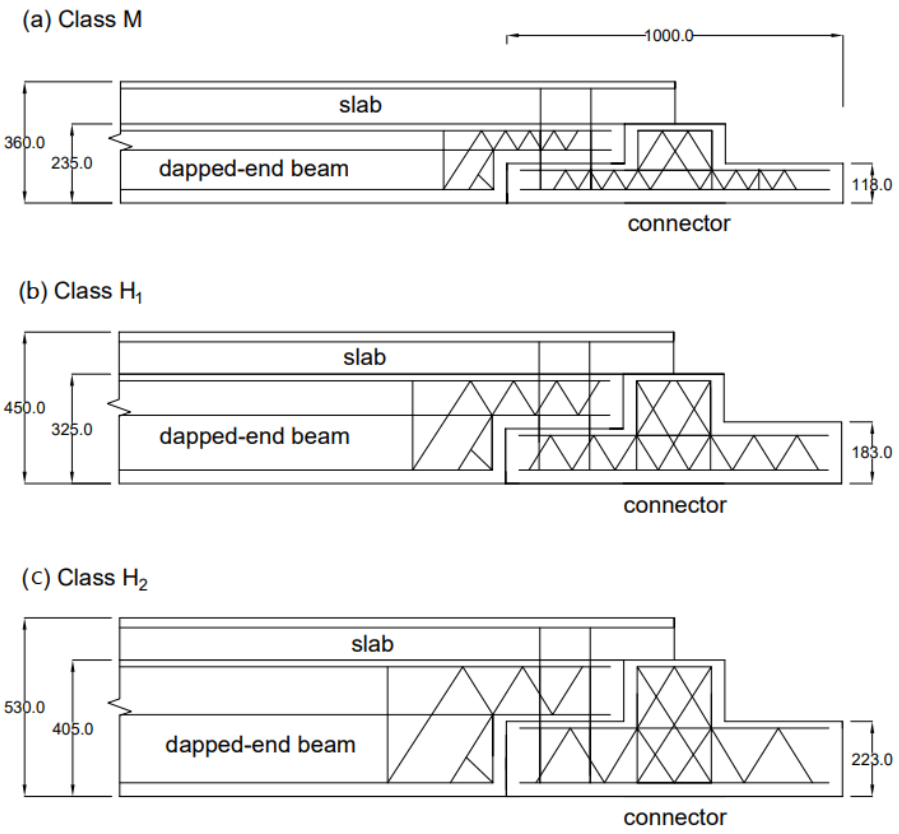

Figure 4. Section view of the developed prefabricated footing systems for (**a**) Class M/M-D, (**b**) Class H_1/H_1-D, and (**c**) Class H_2/H_2-D (length in mm).

Table 2. Sections of the developed prefabricated footing system for each site class.

Class	Type	B_w (mm)	D (mm)	L (m)	No. of Beams	EI/L
M/	waffle raft	110	310	15	13	8.5
M-D	prefabricated	300	360	15	4	8.5
H_1/	waffle raft	110	385	15	13	8.8
H_1-D	prefabricated	300	450	15	4	8.8
H_2/	waffle raft	110	460	15	13	9.0
H_2-D	prefabricated	300	530	15	4	9.0

2.2. Structural Performance Using a Hydromechanical Model

An advanced three-dimensional coupled hydromechanical finite element model, developed and validated by Teodosio et al. [18,27], was used to investigate the structural performance of a prefabricated footing system. Fluid diffusion in an isotropic porous soil medium was modelled as [28,29]:

$$k_{sat}S^3\psi_w\left[\frac{\partial}{\partial x}\left(\frac{\partial h}{\partial x}\right)+\frac{\partial}{\partial y}\left(\frac{\partial h}{\partial y}\right)+\frac{\partial}{\partial z}\left(\frac{\partial h}{\partial z}\right)\right]=m_{sw}\gamma_w\frac{\partial h}{\partial t}, \quad (3)$$

where k_{sat} is the fully-saturated soil permeability, S is the soil saturation, ψ_w is the pore water pressure or soil suction, h is the water potential head, m_{sw} is the slope of the soil–water characteristic curve (SWCC), γ_w is the unit weight of water and t is time.

The hydromechanical behaviour of reactive soils was described as [18,30,31]:

$$d\sigma' = E[\varepsilon_{es}+\varepsilon_{ms}] = E\left[\frac{\kappa}{1+e_0}d\left(ln\left(\frac{\sigma^{eq}}{\sigma_0^{eq}}\right)\right)+\frac{1}{3}\left(d\varepsilon'_{ms}\frac{dS}{d\psi_w}d\psi_w\right)\right], \quad (4)$$

where σ' is the soil effective stress, E is the elastic constant soil tensor, ε_{es} is the soil effective stress–strain and ε_{ms} is the moisture swelling soil strain, κ is the logarithmic soil bulk modulus, e_0 is the initial soil void ratio, σ^{eq} is the final equivalent pressure based on the three-dimensional orthogonal stresses, and σ_0^{eq} is the initial equivalent pressure.

The model used to consider concrete tensile cracking and concrete compressive crushing was the Concrete Damaged Plasticity (CDP) model [32]. The stress–strain curve shows a linear elastic relationship through σ_{t0} and σ_{c0} for uniaxial tension and compression. Surpassing the value of σ_{t0} represent the failure stresses where the formation of cracking occurs due to the softening response from the stress–strain relationship causing strain localisation in concrete elements. Surpassing the value of σ_{c0} yet less than the ultimate compression stress, σ_{cu}, represent the failure stresses with hardening response of the stress–strain curves. Contrarily, beyond the value of σ_{cu} reflects the crushing of concrete with a softening response.

The contact element approach is employed for the interaction between reactive soils and footing systems. This method allows the soil–structure contact and separation with consideration of the tangential behaviour and normal behaviour. A more detailed discussion of the CDP model and contact elements are discussed in Dassault Systèmes [33].

Stopping criterion of the developed model for all simulations was based on Standards Australia [24]. A surface pore pressure, u, was specified as a boundary condition and continuously applied to the open ground. The simulation was then terminated when a change in u below the active depth zone, H_s, had eventuated.

The list of parameter inputs for the numerical simulations of the developed prefabricated footing systems and the monolithic waffle rafts are presented in Table 3. Details of the numerical simulations are presented in Appendix A.

Table 3. Parameter inputs for the numerical simulations of prefabricated footings and waffle rafts related to soil state, environmental factors, footing dimensions and stress condition.

Notation Soil Parameters	Parameter	Value	References
ρ_b	soil density	1550 to	[34]
κ	log bulk modulus	0.05 (swell) 0.03 (shrink)	[35], [30] [36] [37]
ν_{soil}	soil Poisson's ratio	0.45 (swell) 0.1 (shrink)	[38]
ε_{ms} vs. S	moisture-swelling curve	8%	[34], [38]
k_{sat}	saturated permeability	1×10^{-7} to 1×10^{-9} ms^{-1}	[34], [39]
ψ_w vs. S	sorption curve	-1×10^{1} to -1×10^{5} kPa	[34], [18]
Environmental Parameters			
$\Delta\overline{u}$	average suction change	1.2 pF	[24]
H_s	active depth zone	3.0 m	[24]
Footing and Stress Parameters			
p	area load	2.5 kN m^{-2}	[40], [41]
q	line load	6.5 kN m^{-1}	[40], [41]
μ	coefficient of friction	0.35 (soil-concrete) 0.4 (concrete-concrete)	[42], [38]
E_c	concrete elastic modulus	40 GPa	[43], [24]
ν_c	concrete Poisson's ratio	0.2	[43], [38]
E_s	steel elastic modulus	450 GPa	[43], [27]
ν_s	steel Poisson's ratio	0.3	[43], [27]

2.3. Life Cycle Cost Analysis

The Life Cycle Cost (LCC) analysis was based on AC11093144 [44] to compare the overall life cycle cost of the developed prefabricated footing systems and the monolithic waffle rafts. The LCC estimates include construction and disposal costs. This study assumed that operation and occupancy costs are negligible. Present values were calculated from future costs by applying discounts. The LCC is described as

$$\text{LCC} = C_C + C_D, \tag{5}$$

where C_C is the construction cost and C_D is the disposal or end-of-life cost. To effectively calculate the values of LCC for each footing system, the present value of C_D can be estimated using

$$C_D^{PV} = \frac{C_D^{FC}}{(1+d_r)^{t_d}}, \tag{6}$$

where C_D^{PV} is the present value of the disposal cost, C_D^{FC} is the future cost of the disposal cost, d_r is the discount rate and t_d is the structure deployment period in years.

The scale of the projects affects the calculated values of LCC. Based on past studies, the scale of a specific project determines whether a prefabricated solution will be pragmatic or

uneconomical [45,46]. To consider the different scale of projects and assess the applicability of the developed prefabricated footing systems, cost analyses focusing on the comparison of material consumption and life cycle costs (LCC) are performed. These cost analyses determine the practicality of the developed prefabricated footing systems where the values of LCC are comparable or more economical to the values of the specific monolithic waffle rafts through varying the project floor area, A_f, and structure deployment period, t_d, for each site classification (i.e., Classes M-D, H_1-D and H_2-D). Equation for LCC can then be described as:

$$\text{LCC} = \left[C_{fc} + \sum(C_{dc})(A_f) + \sum(C_{ic})(t_c)\right] + \frac{C_D^{FC}}{(1+d_r)^{t_d}}, \quad (7)$$

where C_{fc} is the fixed costs, C_{dc} is the direct costs proportional to the slab floor area A_f, C_{ic} is the indirect costs proportional to the construction period, and t_c is the duration of construction.

Construction costs were derived from Rawlinsons [47], a primary reference for the AEC industry. Other resources, such as case studies, construction quotes and subcontractor estimates, were used when data were unavailable in the primary reference. Sample estimates to calculate the values of LCC for the developed prefabricated footing systems and the monolithic waffle rafts are presented in Tables 4 and 5, respectively.

Specific assumptions for the LCC analyses of the developed prefabricated footing systems were made. First, the site mobilisation cost was taken from Rawlinson's Cost Guide [47] and advice from abuilding subcontractor based in Melbourne, which was assumed to be constant for both prefabricated systems and cast-in-place waffle rafts. Second, supplies of flexural, shear and mesh reinforcements were extracted from Rawlinsons [47], which include delivery costs. Third, concrete wastage is negligible since the prefabricated systems will be manufactured in a controlled environment. Lastly, labour productivity was based on Rawlinson's Cost Guide [47] and engineering inspections were not included.

Table 4. LCC estimate for the developed prefabricated footing with a floor area, A_f, of 225 m^2 on a Class H_2/H_2-D soil deployed for t_d = 50 years.

Item	Description	Qty	Unit	Rate (AUD)	Amount (AUD)
A	**Site preparation**				
A1	Slab set-out	1	Item	600.00	600.00
A2	Mobilisation and float costs	1	Item	900.00	900.00
A3	Removal of vegetation and ground leveling	225	m^2	2.14	481.50
A4	Site soil compaction	225	m^2	1.85	416.25
A5	Installation/removal of fencing	60	Lm	42.00	2520.00
B	**Formwork and reinforcement**				
B1	Steel reinforcement (Beam)	1.34	t	2260.00	3020.65
B2	Mesh (Slab)	0.81	t	2260.00	1836.00
B3	M20 dowel	192	Item	11.88	2280.96
B4	Plant (form release/installation)	11.63	hr	63.00	732.58
C	**Concrete work**				
C1	Concrete mix	42.71	m^3	200.00	8541.00
C2	Manufacturing plant processes	26.69	hr	60.50	1614.78
D	**Delivery and installation**				
D1	Float of prefabricated elements to site	10,462.73	t km	0.09	941.65
D2	Mobilisation of crane	1	Item	500.00	500.00
D3	Crane hire (+ operator/fuel)	14.40	hr	220.00	3168.00
D4	Tradesman (+ lifting/installation)	28.8	hr	63.00	1814.40
E	**Miscellaneous**				
E1	Concrete batching plant overheads (20 % of construction cost)	1	Item	3237.99	3237.99
E2	Drawings	36	Item	63.89	2300.00
E3	HSE Plan	1	Item	1500.00	1500.00
F	**End of life**				
F1	Mobilisation of crane	2	Item	500.00	1000.00
F2	HSE Plan	1	Item	1500.00	1500.00
F3	Crane hire (+ operator/fuel)	28.80	hr	220.00	6336.00
F4	Tradesman	57.6	hr	63.00	3628.80
TOTAL LCC					**53,157.06**

Assumptions to calculate the total values of LCC of the cast-in-situ monolithic waffle rafts include, first, the site preparation cost, and reinforcements and labour productivity were based on Rawlinsons [47], similar to the assumptions for the developed prefabricated systems. Second, the estimated cost of expanded polystyrene (EPS) for the cast-in-situ monolithic waffle rafts was quoted by a supplier based in Melbourne with an assumption of a 10% provisional cost for wastage. Third, the supply of concrete and concrete pouring cost was based on Rawlinson's Cost Guide [47] with an added 15% as a contingency.

Table 5. LCC estimate for the monolithic waffle raft with a floor area, A_f, of 225 m^2 on a Class H_2/H_2-D soil deployed for t_d = 50 years.

Item	Description	Qty	Unit	Rate (AUD)	Amount (AUD)
A	**Site preparation**				
A1	Slab set-out	1	Item	600.00	600.00
A2	Mobilisation and float costs	1	Item	900.00	900.00
A3	Removal of vegetation and ground leveling	225	m^2	2.14	481.50
A4	Site soil compaction	225	m^2	1.85	416.25
A5	Installation (+ removal) of fencing	60	Lm	42.00	2520.00
B	**Formwork and reinforcement**				
B1	Steel reinforcement (Beam)	0.80	t	2260.00	3020.65
B2	Mesh (Slab)	0.81	t	2260.00	1836.00
B3	Formwork	60	Lm	30.00	1800.00
B4	Waffle pods	163	No.	10.00	1630.00
B5	Tradesman (placing and tie)	17.55	hr	63.00	1106.00
B6	Tradesman (+ formwork)	17.4	hr	63.00	1096.20
B7	Labourer	6	hr	60.50	350.30
C	**Concrete pour**				
C1	Concrete (+ delivery truck)	43.18	m^3	200.00	8636.06
C2	Concrete pumping	43.18	hr	8.00	345.44
C3	Labourer (pour/vibration/finish)	47	hr	60.50	2839.57
E	**End of life**				
E1	Demobilisation (break-up/removal)	225	m^2	90.00	20,250.00
TOTAL LCC					**48,244.27**

2.4. Life Cycle Assessment

As an environmental sustainability criterion, this study performed life cycle energy and GHG emissions for the developed prefabricated footing systems and the cast-in-situ monolithic waffle rafts. For this, this study quantified total energy consumption and GHG emissions throughout the entire life cycle stages, from product production (A1–A3), transport to the site (A4), construction (or installation, A5), and deconstruction (C1). This study does not take into account the energy consumption or GHG emissions resulting from the use of both systems. The life cycle boundaries based on EN15978 [48] for both footing systems are shown in Figure 5.

The quantification of the lifecycle energy and GHG emissions based on the system boundary shown in Figure 4 is as follows.

$$\text{Lifecycle Energy} = \sum_{i=1}^{1} EE_M(Comp)_i + \sum_{i=1}^{1} EE_T(Comp)_i + \sum_{i=1}^{1} EE_C(Comp)_i + \sum_{i=1}^{1} EE_D(Comp)_i + \sum_{i=1}^{1} EE_R(Comp)_i, \quad (8)$$

$$\text{Lifecycle GHG} = \sum_{i=1}^{1} EC_M(Comp)_i + \sum_{i=1}^{1} EC_T(Comp)_i + \sum_{i=1}^{1} EC_C(Comp)_i + \sum_{i=1}^{1} EC_D(Comp)_i + \sum_{i=1}^{1} EC_R(Comp)_i, \quad (9)$$

where, EE_M: Embodied energy of material (MJ), (Comp)*i*: is a particular component i = 1, 2, 3 and so forth, EE_T: Embodied energy due to transport to site, EE_C: Embodied Energy

due to construction, EE_D: Embodied energy due to demolition, EE_R: Embodied energy due to reuse/recycling, and EC: Embodied GHG. Embodied energy and GHG data for each construction product and component (A1–A3 in Figure 4 and EE_M: in Equation (9)) were used the values in the EPiC database [49], which is open access environmental flow database for Australian building products [50], and data not provided in the EPiC database were used using the Australian national LCI (AusLCI) database.

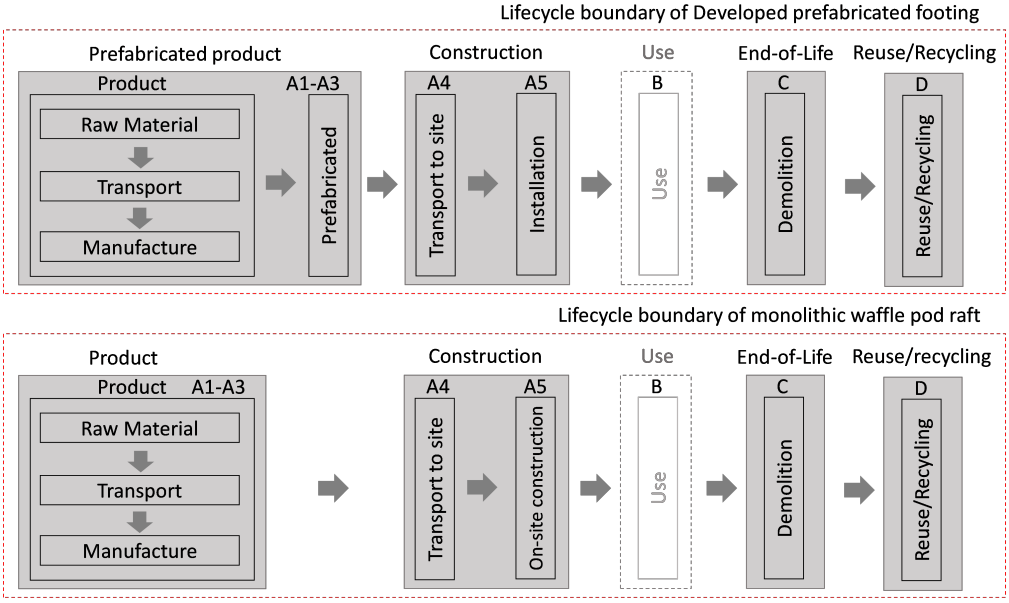

Figure 5. Life cycle boundaries of two footing systems.

In this study, it is assumed that a gantry crane is used in a prefabricated manufacturing plant where concrete is poured into molds and modules are loaded onto trucks (i.e., handling and transportation). The energy consumption and GHG emissions associated with the transport of products (components) to the site (A4 in Figure 4 and EE_T, EC_T in Equations (9) and (10)) may vary depending on the type and size of transport and the distance transported. This study assumes that the transport of construction products (components) is transported by 15–18 tonne trucks, and the distance is assumed to be 50 km, which is the round-trip distance of metropolitan area in Australia.

Energy consumption and the resulting GHG emissions due to construction or assembly at the site (EE_C & EC_C in Equations (9) and (10)) may vary depending on the equipment operation skill level of the site worker or the site conditions. The effects of the use of equipment during construction were considered to be only the energy and carbon emissions resulting from the use of major equipment such as excavators for on-site cutting or mobile cranes for the assembly of prefabricated footing systems. In this study, the energy and carbon emission values according to the use of on-site equipment were obtained from the literature and are summarised in Table 6.

In addition, the effects of the deconstruction of a building that has reached the end of its service life were applied to this study by calculating the energy consumption and GHG emission values of the concrete structure demolition, which were obtained from the literature. In this study, the benefits for the reuse and recycling of the both footing systems after deconstruction were also considered. The prefabricated footing systems can be disassembled and transported for use on another construction site. The prefabricated footing systems are assumed to be reusable after the structure deployment period (t_d) or after the life of the structure. On the other hand, the cast-in-place monolithic waffle rafts were assumed to be recyclable by recovering the reinforced steel rebar after deconstruction the structure.

The energy and carbon emission factors are summarised in Table 6.

Table 6. Energy and GHG emission factors used for life cycle assessment of both footing system.

Item by Life Cycle	Unit	Energy (MJ Unit^{-1})	GHG (kg CO_2e Unit^{-1})	References
Construction (A)				
Concrete (32 MPa)	m^3	2776.00	412.00	[50]
Hot-rolled steel	kg	30.60	2.40	[50]
Gantry crane	hr	190.60	14.10	[51]
Transportation (A4, C2)				
Truck (15–30 tonne)	tkm	2.71	0.203	[50]
Excavator (0.2 m^3 bucket)	tkm	0.74	0.053	[51]
Mobile crane (50 ton)	hr	190.60	14.10	[51]
Construction				
Excavator	MJ/hr	107.50	13.12	[51]
Concrete pump	hr	1094.30	81.40	[52]
Mobile crane	hr	190.60	14.20	[51]
End of life				
Concrete demolition (C)	kg	0.007	0.00054	[50]
Recycling aggregates	kg	0.07	0.006	[50]
Recycling steel	kg	11	0.74	[50]
Benefit by recycling (D)				
Recycled aggregates	kg	−0.213	−0.0169	[50]
Recycling steel	kg	−30.3	−2.4	[50]

3. Results and Discussion

The global performance of the developed prefabricated footing systems were investigated using a multi-criteria analysis incorporating: (1) the structural performance using a coupled hydromechanical finite element model by [18]; (2) licycle cost analysis; and (3) life cycle assessment considering energy and GHG. The results of the multi-criteria analysis are outlined below.

3.1. Structural Performance

To provide an effective comparison of the structural performance of each footing system, the substructures were exposed to varying soil movements (y_s) for both edge heaving scenarios (Figure 1a) and centre heaving scenarios (Figure 1b).

The developed prefabricated footing systems with the three components: (1) the developed DEB and bolt connection; (2) the connectors for dimensional coordination; and (3) the slab deck, presented in Figures 3 and 4. The global performance of the developed prefabricated footing systems was compared to monolithic waffle rafts taking into account soil reactivity site classification outlined in Table 1. The dimensions of the footing systems are described in Table 2, with similar unit stiffness and constant floor area (15 m by 15 m) to effectively compare the two types of substructures.

The shrink–swell soil movement induced footing system deformation through soil–structure interaction. Results of the numerical simulations are presented in Figure 6 for swelling soils and in Figure 7 for shrinking soils.

In swelling soils, both footing systems were lifted by the heaving uncovered ground around the perimeter of the substructure (Figure 6). This soil–structure interaction response was sensible since both footing systems were designed to be constructed on-ground without any embedded beams. The developed prefabricated footing systems for each site class (i.e., M/M-D, H_1/H_1-D and H_2/H_2-D) transferred the forces and moments effectively, which led to a continuous footing deformation. Furthermore, the components of the developed prefabricated footings were functionally integrated together causing the whole system to act as simply-supported elements. Comparing both footing systems, the developed prefabricated footings were more suspended than the monolithic waffle rafts specifically when y_s had higher values (Figure 6c,e). This was due to a thicker slab deck that makes the

prefabricated system resist more applied area loads comparable to suspended structural elements. However, the prefabricated system requires a relatively greater amount of concrete due to the increased slab thickness.

In shrinking soils, both footing systems acted like cantilever structures shown in Figure 7. The footing systems curved outwardly due to the applied line loads at the perimeter edges. The developed prefabricated footing systems also performed homogeneously similar to the swelling scenario. This reflects the continuous transfer of forces and moments in the entire substructure. Moreover, the total footing deformation was less than that of the monolithic waffle rafts where the largest displacements were experienced at the corner of the substructures.

The developed prefabricated footing system observed generally lower structural deformation induced by the swelling soil and shrinking soil, as outlined in Table 7. Assuming a superstructure made up of an articulated masonry veneer for all simulations, the allowable deformation (Δ_{max}) for the footing systems was 30 mm based on Standards Australia [24]. The developed prefabricated footing system obtained an acceptable deformation for both swelling and shrinking scenarios when the site classification was M/M-D ($30 < y_s \leq 45$ mm). Contrarily, the monolithic waffle raft on Class M/M-D site exceeded Δ_{max} when the soil was shrinking. Both footing systems had exceeded Δ_{max} when the site classifications were H_1/H_1-D and H_2/H_2-D ($y_s > 45$ mm). However, the monolithic waffle rafts had significantly greater structural deformation than the developed prefabricated systems. Moreover, changing the assumption of the type of superstructure construction to cladding, instead of an articulated masonry veneer, may obtain acceptable structural deformation for the developed prefabricated systems since the value of Δ_{max} will change to 40 mm. This is unlikely for the monolithic waffle rafts where the values of structural deformation are more than the limit.

Table 7. Deformation, Δ, of footing systems on shrinking and swelling soil considering site classification based on soil surface characteristic movement, y_s in millimetres Standards Australia [24].

Class	Scenario	Prefabricated Footing				Waffle Raft			
		y_s = 30 (mm)	y_s = 45 (mm)	y_s = 60 (mm)	y_s = 75 (mm)	y_s = 30 (mm)	y_s = 45 (mm)	y_s = 60 (mm)	y_s = 75 (mm)
M/ M-D	swell	23	25	-	-	25	33	-	-
	shrink	25	27	-	-	25	39	-	-
H_1/ H_1-D	swell	-	22	25	-	-	33	43	-
	shrink	-	27	38	-	-	39	51	-
H_2/ H_2-D	swell	-	-	36	39	-	-	38	48
	shrink	-	-	32	39	-	-	42	63

The monolithic waffle rafts deformed excessively specifically when experiencing shrinking ground motion. The monolithic waffle rafts, based on the numerical simulations [27], do not perform satisfactorily on shrinking soil due to insufficient top reinforcing steel bars. The main flexural reinforcements were located at the bottom portion as stipulated in Standards Australia [24]. These recommended design specifications do not fully consider the behaviour of monolithic waffle rafts when acting as double cantilevers (Figure 1b) when uncovered soils are shrinking. This shrinking scenario causes negative moment in the substructure, where the only resisting reinforcements are the meshes of slabs.

The possible reasons that caused the footing system to experience system deformation more than Δ_{max} are, first, the calculated EI/L from the recommended design in Standards Australia [24] may have been underestimated. This recommended design was based on the analysis using the Walsh Method, an uncoupled two-dimensional approach discussed in [27]. Secondly, due to the approach used in the design standard (i.e., AS 2870-2011), consideration of the non-linear behaviour and plastic mechanisms of soil, concrete and steel were not considered. Lastly, since the approach used in the design standard was two-dimensional, the critical values at the re-entrant corners (Figures 6 and 7) may have not been considered thoroughly.

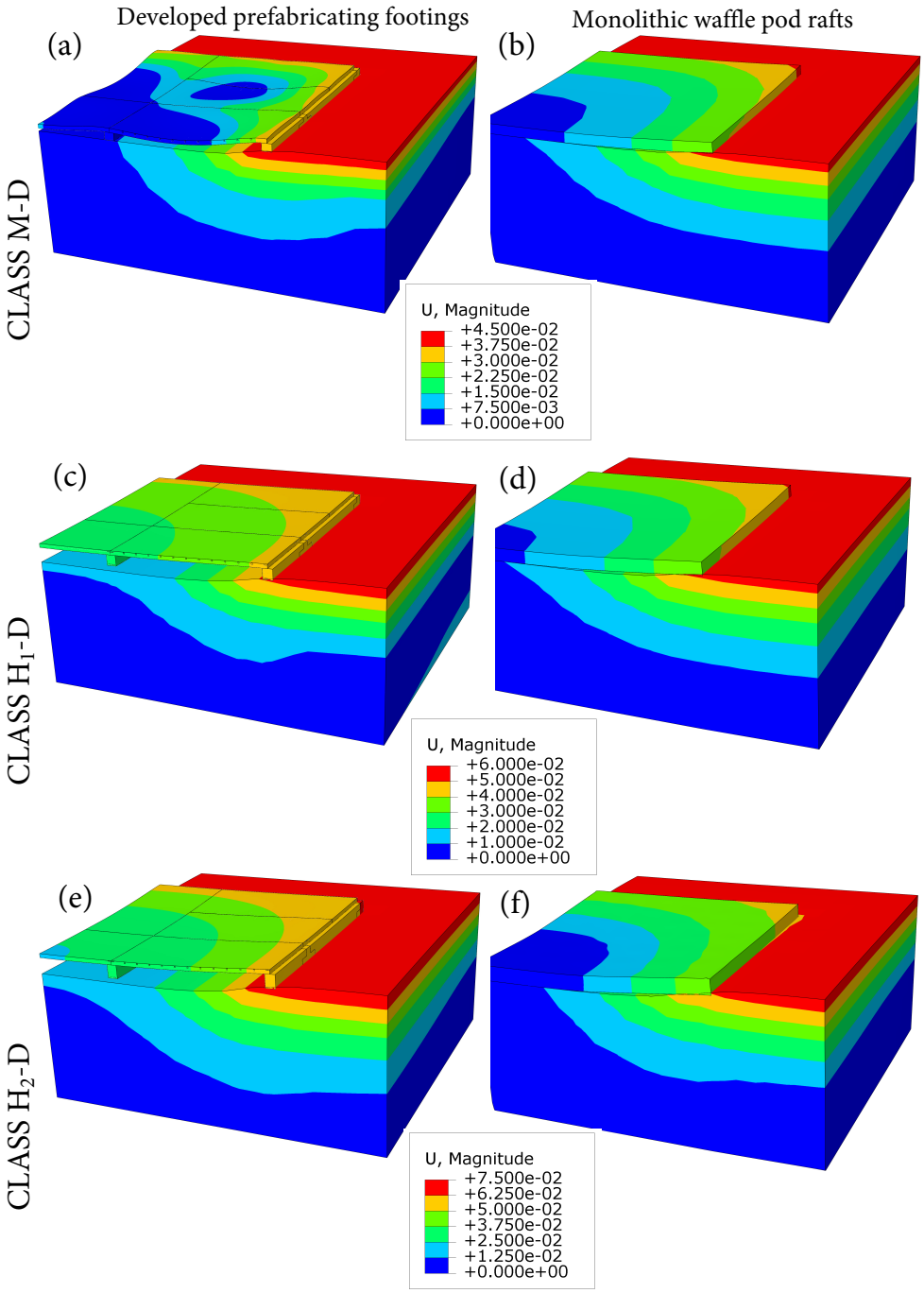

Figure 6. Comparison of swelling soil movement and footing deformation between the developed prefabricated footing systems and waffle rafts for (**a**,**b**) Class M-D soil, (**c**,**d**) Class H_1-D soil, and (**e**,**f**) Class H_2-D soil. Values of displacements are in metre.

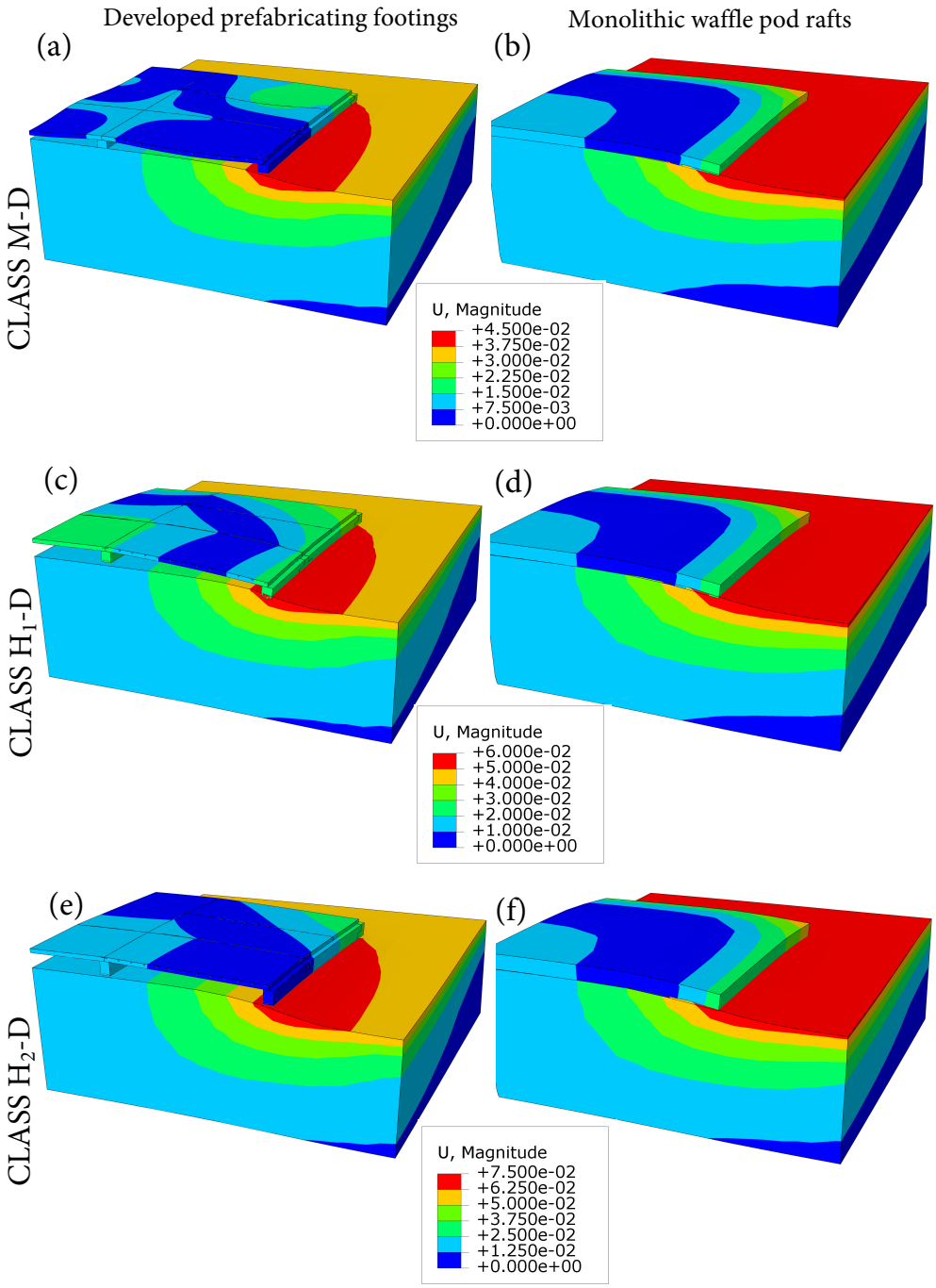

Figure 7. Comparison of shrinking soil movement and footing deformation between the developed prefabricated footing systems and waffle rafts for (**a**,**b**) Class M-D soil, (**c**,**d**) Class H_1-D soil, and (**e**,**f**) Class H_2-D soil. Values of displacements are in metre.

The edge heave and centre heave cracking damage (d_t or DAMAGET) to the developed prefabricated footings and the monolithic waffle rafts are presented in Appendix B. The prefabricated system mostly experienced the structural damage in the DEB element, which is desirable since the connection was transferring the forces and moments effectively. In the edge heave scenario, the monolithic waffle raft experienced most structural damage close to the centre of the entire footing system, which is logical since the centre is the critical area for suspended structural elements. Figure A4 shows the yielding of steel. It can be observed that the yielding of steel in the prefabricated systems and the monolithic waffle rafts were in a similar area to where the simulated cracking propagated. In the

centre heave scenario, the developed prefabricated footing systems for highly reactive sites had localised structural damage around the bolt connections. This indicates that, when the line loads were applied onto the prefabricated footing systems acting as a cantilever, the bolt connection and steel reinforcements moved outwardly and yielded due to the negative moment experienced by the systems. Thus, the governing failure was around the bolt connections keeping the whole prefabricated systems intact and jointed. To mitigate this, a perimeter piling can be installed. On the other hand, extensive structural damage was observed in the monolithic waffle rafts for highly reactive sites. Severe structural damage was experienced close to the perimeter, which was around the second to third internal beams from the edge beams. This was due to the lack of reinforcements to resist the negative moment, which only relied on the mesh of the slab.

The structural performance of the developed prefabricated system using a finite element method was found to have better structural performance than the conventional waffle raft, with up to 40% reduced footing deformation. Furthermore, the prefabricated system had reduced concrete cracking due to the material layout designed for both positive and negative bending moment considering the swelling and shrinking of reactive soils.

3.2. Life Cycle Cost Analysis

The structural performance of the developed prefabricated footing systems for different site classifications (Site Classes M/M-D, H_1/H_1-D and H_2/H_2-D) was more adequate than the monolithic waffle rafts based on the numerical simulations. However, the quantity of concrete and steel materials used in the design should also be considered for an effective comparison. Table 8 outlines the total material quantity used for the footing systems with respect to each site classification. The amount of concrete used for the developed prefabricated system for each site class ranged from 32 to 38 m^3, comparable to that of the monolithic waffle rafts which ranged from 30 to 38 m^3. Most of the difference in concrete consumption was due to the thickness of the slab between the developed prefabricated systems, equal to 125 mm, and the monolithic waffle rafts, equal to 85 mm. A thicker slab of the developed prefabricated footings was necessary to prevent excessive deformation. Steel reinforcements for the prefabricated footing systems were 350 to 630 kg greater than the reinforcements in the waffle rafts. This was due to the required steel reinforcements in the D-region portions of the connections and the top flexural reinforcements to resist negative bending moments.

The values of LCC were estimated for each site using Equation (7) for the footing systems on varying soil classifications (Figure 8). The estimates show that the values of LCC for the cast-in-place monolithic waffle rafts were consistently lower than the values of LCC for the developed prefabricated footing systems. This construction cost difference was mainly due to the consumed materials, specifically for the supply of concrete and steel reinforcements. However, the percentage difference of LCC between the footing systems can be minimised. Based on Figure 8, the percentage difference of LCC between the two systems can be reduced to 6% when the prefabricated system was installed in a highly reactive site with larger A_f.

The cost analysis observed that dwellings having larger A_f assembled on very highly reactive soil can be cost-competitive averse to cast-in-place waffle rafts.

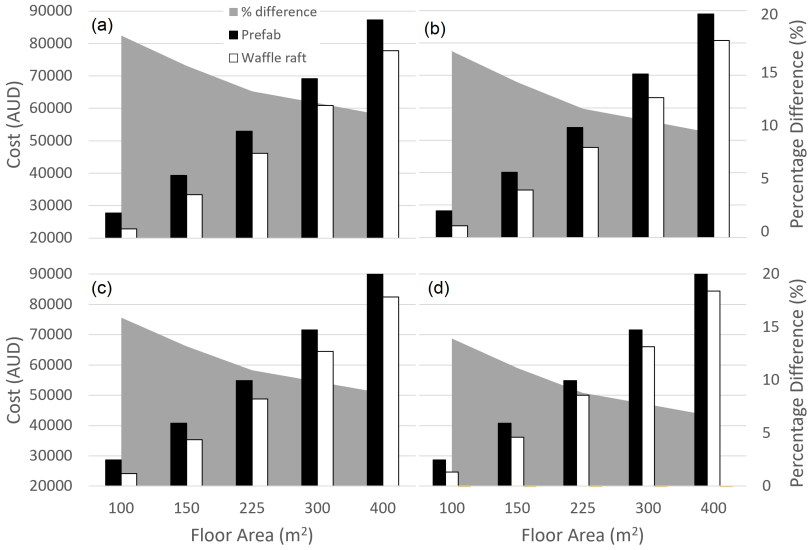

Figure 8. Comparison of the Life Cycle Cost analysis between the prefabricated system and waffle raftsfor each site classification, (**a**) Class M/M-D, (**b**) Class H_1/H_1-D, (**c**) Class H_2, and (**d**) Class H_2-D.

Table 8. Material quantity survey of the developed prefabricated footings systems and the monolithic waffle rafts.

	Prefabricated Footings			Waffle Rafts		
M/M-D Concrete	**Section Vol. (m^3/unit)**	**Number (unit)**	**Vol. (m^3/unit)**	**Section Vol. (m^3/unit)**	**Number (unit)**	**Vol. (m^3/unit)**
Beams	0.50	8	3.96	0.85	13	11.05
Slabs	28.13	1	28.13	19.13	1	19.13
Total			32.09			30.18
Steel	Diameter (m^2)	Length (m)	Mass (kg)	Diameter (m^2)	Length (m)	Mass (kg)
Flexural	0.000491	1234.21	522	0.000113	390.00	449
Shear	0.000201	159.36	243	-	-	-
Mesh	0.000050	2250.00	625	0.000038	2250.00	625
Bolts	0.000314	57.60	16	-	-	-
Plates	0.001100	12.00	8	-	-	-
Total			1424			1074
H_1/H_1-D Concrete	Section vol. (m^3/unit)	Number (unit)	Vol. (m^3)	Section vol. (m^3/unit)	Number (unit)	Vol. (m^3)
Beams	0.90	8	7.20	1.13	13	14.70
Slabs	28.13	1	28.13	19.13	1	19.13
Total			35.33			33.83
Steel	Diameter (m^2)	Length (m)	Mass (kg)	Diameter (m^2)	Length (m)	Mass (kg)
Flexural	0.000491	1706.89	722	0.000113	390.00	449
Shear	0.000201	220.39	336	-	-	-
Mesh	0.000050	2250.00	813	0.000050	2250.00	813
Bolts	0.000314	57.60	16	-	-	-
Plates	0.001100	12.00	8	-	-	-
Total			1895			1262
H_2/H_2-D Concrete	Section vol. (m^3/unit)	Number (unit)	Vol. (m^3)	Section vol. (m^3/unit)	Number (unit)	Vol. (m^3)
Beams	1.26	8	10.08	0.76/1.42	13	14.70/18.42
Slabs	28.13	1	28.13	19.13	1	19.13
Total			38.21			33.83/37.55
Steel	Diameter (m^2)	Length (m)	Mass (kg)	Diameter (m^2)	Length (m)	Mass (kg)
Flexural	0.000491	2127.04	890	0.000201	390.00	798
Shear	0.000201	274.64	419	-	-	-
Mesh	0.000050	2250.00	625	0.000050	2250.00	625
Bolts	0.000314	57.60	16	-	-	-
Plates	0.001100	12.00	8	-	-	-
Total			1959			1423

3.3. Life Cycle Assessment: Energy and Ghg

The life cycle energy and GHG emissions of two footing systems (prefabricated footing systems and on-site waffle rafts) are presented in Figure 9. Energy consumptions and GHG emissions of the two systems are divided into four stages according to EN15978 [48]. Each of these stages includes material production (A1–A3), construction (A4–A5), end-of-life (C) and recycling/recovery (D) or Reuse (D(reuse)).

Energy consumption in the material production occupies about 75% of the total, and GHG emissions occupy 84% of the total, indicating that more than three quarters of the total energy and GHG emissions occur in the material production stage (Figure 9). Prefabricated footing systems use relatively higher amounts of concrete (approximately 2–6% higher depending on each site classification) and steel (33–50%) compared to waffle rafts (see Table 8). This causes an increase in energy and GHG emissions for product production (stage A) of the prefabricated footing systems. As shown in Figure 9, the GHG emissions of the product production (stage A) of the prefabricated footing systems is about 8–18%, and the energy consumption is about 12–21% more depending on each site classification (Figure 9).

The energy and GHG emissions due to transport of necessary materials (stage A4) are dependent on the distance from manufacturing plants to construction sites. In the prefabricated footing systems, the transport distance may be longer than the onsite waffle rafts because the material should be considered from the manufacturing plant to the prefabrication plant and to the construction site. This can cause an increase in energy consumption and corresponding GHG emissions due to transport of materials and products. Transport impact of prefabricated footing systems (A4 stage) was 2% to 13% higher (depending on each site classification) than that of on-site waffle pods systems (Figure 9). However, the impact of transportation is less than 5% of the total, and this difference is insignificant in the overall life cycle impact (Figure 9).

In terms of energy consumption and GHG emissions due to the use of equipment on the site, the prefabricated footing systems are shown to be relatively superior, having 18% to 22% less GHG emissions compared to on-site waffle pods systems (Figure 9b,d). However, the impact of energy and GHG emissions due to construction (stage A5) was found to be insignificant, contributing only 1% (GHG emissions) or 2% (energy consumption) of the total impact.

End-of-life stage (stage C) includes deconstruction, transportation and processing of waste. The impact of this stage C on overall energy and GHG emissions does not differ significantly between the two footing systems. GHG emissions at this stage was found to account for 11–12% of the total in both systems, and energy consumption was found to account for 17–18% of the total. Between the two footing systems, the prefabricated system has 17–24% more GHG emissions and 18–25% more energy consumption compared to the on-site waffle rafts. This is because the prefabricated footing systems use relatively more material compared to on-site waffle rafts (as shown in Table 8), therefore energy and GHG emissions from deconstruction and waste disposal stages are also correspondingly higher.

Recycle or recovery of material (stage D) represents benefits obtained from the recycling and recovering of waste. Recently, this stage has gained growing attention because reuse and recycling do not only reduce construction waste sent to landfills but also decrease raw materials used for new construction. In this study, this stage was analysed into two cases; the recycling of concrete and steel (represented as stage D) and the reuse of prefabricated footing systems (denoted as D(reused)) in Figure 9. Energy and GHG emissions were evaluated by dividing the case of recycling into general aggregates or recycled steel through deconstruction like concrete products, and the case of promoting reuse at other construction sites by disassembly and assembly, specifically in the case of the prefabricated system. The energy and GHG reduction effect of the recycling or reuse of each major material/product can be represented as a negative value, and the reduction effect is shown in Figure 9. GHG reduction due to the recycling of concrete and steel is effective from 27% to 35% of the total life cycle GHG emissions, and energy consumption is shown to have the effect of reducing 45% to 57% of total life cycle energy. The prefabricated footing

systems have a carbon reduction effect of about 4% (Class M and H2) to a maximum of 8% (Class H1) more than that of the waffle rafts, and the energy consumption is shown to be reduced by 6% (Class M and H2) to 11% (Class H1), which is more effective than waffle rafts. As shown in Figure 9c,d, stage D was closely related to stage A and C. Since the prefabricated systems require a relatively large amount of material compared to waffle rafts, energy consumption and GHG emissions for deconstruction and waste processing were relatively higher than that of the waffle rafts (stage C in Figure 9). On the other hand, the benefit from the recycling of waste was also higher in the prefabricated footing system compared to the waffle rafts (stage D in Figure 9) because the amount of waste recycled due to disassembly also increased.

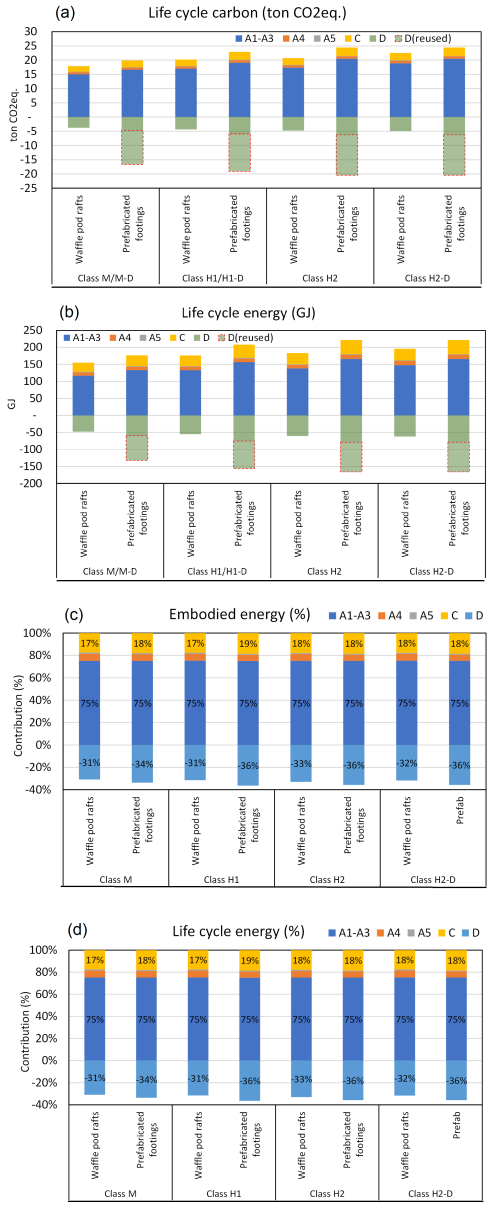

Figure 9. Comparison of the Life Cycle Energy and GHG emissions considering reactive site classification between the developed prefabricated footing systems and waffle rafts ((**a**,**b**) show the amount of GHG emissions and energy consumption according to the life cycle of each stage. 'D(reused)' in (**a**,**b**) represents the energy and GHG reduction effect of the reuse of other sites after disassembly of the prefabricated footing systems). (**c**,**d**) do consider only recycling but do not consider reuse (D(reused)).

In stage D, the prefabricated footing systems can be easily disassembled due to its design for disassembly (DfD), so it can be effectively reused in another site of similar size, as well as for recycling into aggregates or recycled steel. In this case, the reduction effects can be significantly higher because reuse of the prefabricated footing systems reduces material use (stage A) at other construction sites by the same value. In Figure 9a,b, stage D (reused) of the prefabricated footing systems show the carbon and energy reduction effect obtained by reuse at other sites after disassembly. Considering this, the life cycle GHG of the prefab system is about 23% to 25% (23% for M/M-D, 24% for H1/H1-D, 25% for H2 and 23% for H2-D) compared to the waffle pod, and the reduction effect is quite large. The life cycle energy was also found to be about 41%–45% consumed by the prefabricated footing systems (41% of M/M-D, 43% for H1/H1-D, 45% for H2 and 41% for H2-D), which is less than half of the waffle rafts.

Figure 9c,d shows the contribution rate (%) of each stage to the carbon and energy consumption in the life cycle only considering recycle wastes as aggregates and steel.

The life cycle assessment observed that the prefabricated footing systems consume up to 21% more energy for very highly reactive sites, and up to 18% more GHG emissions. When considering the recycling of both footing systems, the difference was less than 10%. Considering the possibility that the prefabricated footing systems can be reused in other sites, the energy and GHG reduction effect is expected to be much greater than that just recycling concrete or steel and, in this case, the GHG is decreased by 75–77% compared to the waffle rafts (55–59% for energy consumption compared to waffle rafts). Thus, the potential energy usage and environmental impact can be significantly compensated for by reusing the prefabricated footing systems.

4. Conclusions

This study investigated the global performance of developed prefabricated footing systems using a multi-criteria analysis for structural performance using FEM, cost efficiency using LCC, and environmental impact using LCA. The developed prefabricated footing systems were compared to cast-in-place monolithic waffle rafts for Site Classes M/M-D, H_1/H_1-D and H_2/H_2-D.

The structural performance was investigated using a three-dimensional hydromechanical FEM. This obtained a more satisfactory global structural performance for the prefabricated footing systems than the traditional cast-in-place monolithic waffle rafts, having the same stiffness for each class site. The prefabricated footing system had reduced deformation and concrete cracking due to the material layout designed for both positive and negative bending moment considering the swelling and shrinking of reactive soils. However, the material consumption of the developed prefabricated footing systems is much greater than that of the cast-in-place waffle rafts. The percentage difference of LCC between the two systems can be reduced to as low as 6% when prefabricated systems were installed in a highly reactive site with larger A_f.

The LCA evaluation, considering only material production, transportation and deconstruction for both systems, observed the prefabricated footing systems to consume up to 21% more energy for Class H_2, and up to 18% more GHG emissions (Class H_2). When considering the recycling of both footing systems after the deconstruction of the building, the prefabricated footing systems still showed high energy consumption and GHG emissions; however, the difference was less than 10%. Considering the possibility that the prefabricated footing systems can be reused in other sites, the energy and GHG reduction effect is expected to be much greater than that of only recycling concrete or steel and, in this case, the GHG is decreased by 75–77% compared to the waffle rafts (55–59% for energy consumption compared to waffle rafts).

From the overall result of the multi-criteria analysis we can observe that the developed prefabricated footing systems can be more advantageous than the conventional in-situ monolithic waffle rafts when prioritising structural robustness, constructing a large house

floor area in a site with a highly reactive classification, and considering potential future substructure reuse.

Author Contributions: Conceptualization, B.T. and F.B.; methodology, B.T. and S.S.; software, P.M.; validation, B.T., F.B. and S.S.; formal analysis, B.T., F.B. and S.S.; investigation, B.T., F.B. and S.S.; resources, K.S.K.B.; data curation, B.T., F.B. and S.S.; writing—original draft preparation, B.T., F.B. and S.S; writing—review and editing, B.T., F.B., K.S.K.B. and S.S.; visualization, B.T., F.B. and S.S; supervision, B.T., K.S.K.B. and P.M.; project administration, B.T., K.S.K.B. and P.M.; funding acquisition, P.M. All authors have read and agreed to the published version of the manuscript.

Funding: The authors would like to thank the Australian Research Council—Centre for Advanced Manufacturing of Prefabricated Housing (ARC-CAMP.H), Industrial Transformation Training Centres—Grant ID: IC150100023 [2015–2018].

Institutional Review Board Statement: Not applicable.

Informed Consent Statement: Not applicable.

Data Availability Statement: Not applicable.

Conflicts of Interest: The authors declare no conflict of interest.

Nomenclature

Structural performance terms and parameters

Notation	Parameter	Notation	Parameter
α	lateral restraint factor	B_w	beam width
α_{sw}, n, m	sorption parameters	D	beam depth
Δ	substructure deformation	DEB	dapped-end beam
Δ_{max}	allowable deformation	d_t, d_c	concrete damage variables
$\Delta\overline{u}$	average suction change	E	elastic modulus
γ_w	unit weight of water	E_c	concrete elastic modulus
κ	logarithmic soil bulk constant	E_s	steel elastic modulus
μ	coefficent of friction	EI/L	Unit stiffness
ν_c	Poisson's ratio of concretel	e_0, e	initial/void ratio
ν_s	Poisson's ratio of steel	FEM	finite element model
ν_{soil}	Poisson's ratio of soil	f_i	other concrete variables
ω	gravimetric soil moisture	f_{k_u}	unsaturated factor
ψ_w	soil suction	G	shear modulus
ρ_b, ρ_w	soil/water bulk density	G_s	specific gravity of solids
σ, σ'	total and effective stress	H_s	active depth zone
$\sigma_0^{eq}, \sigma^{eq}$	initial/equivalent soil stress	H_1/H_1-D	highly reactive soil
σ_t, σ_c	tensile/compressive stress	H_2/H_2-D	very highly reactive soil
σ_{dev}	deviatoric stress	h	water potential head
σ_{t0}, σ_{c0}	tensile/compressive failure σ	h_{soil}	soil layer thickness
θ	volumetric soil moisture	I_{pt}, I_{ss}	instability/shrinkage index
θ_r, θ_s	residual/saturated θ	k_{sat}	saturated conductivity
$\dot{\tilde{\varepsilon}}_t^{pl}, \dot{\tilde{\varepsilon}}_c^{pl}$	equivalent plastic strain rates	k_u	unsaturated conductivity
$\tilde{\varepsilon}_t^{pl}, \tilde{\varepsilon}_c^{pl}$	equivalent plastic strains	L or W	length/width of a footing
ε_{es}	soil effective strain	M/D-D	moderately reactive soil
ε_{ms}	moisture-swelling strain	m_{sw}^2	slope of the sorption curve
ε'_{ms}	test moisture-swelling strain	Q	volumetric water flux
ε_T	simplified total soil strain	S	degree of saturation
$\varepsilon_t, \varepsilon_c$	elastic concrete strains	T_m	temperature of concrete
$\varepsilon_t^{pl}, \varepsilon_c^{pl}$	plastic concrete strains	y_s	expected soil movement

Cost analysis terms and parameters

Notation	Parameter	Notation	Parameter
A_f	floor area	C_{fc}	fixed cost
C_C	construction cost	C_{ic}	indirect cost
C_D	disposal cost	d_r	discount rate
C_D^{PV}	present value of disposal cost	LCC	life cycle cost
C_D^{FV}	future value of disposal cost	t_c	construction duration
C_{dc}	direct cost	t_d	structure deployment period

Sustainability assessment terms and parameters

Notation	Parameter	Notation	Parameter
EC_C	construction embodied GHG	EE_C	construction embodied energy
EC_D	demolition embodied GHG	EE_D	demolition embodied energy
EC_M	material embodied GHG	EE_M	material embodied energy
EC_R	reuse/recycling GHG	EE_R	reuse/recycling energy
EC_T	transportation GHG	EE_T	transportation energy
LCA	life cycle assessment	LCI	life cycle inventory

Appendix A. Details of the Numerical Simulations Using the Hydromechanical Model by Teodosio et al.

Appendix A.1. Simplified Hydromechanical Finite Element Model

A reactive soil mass is modelled as a three-phase elastic material to analyse an unsaturated porous medium. The soil mass consists of solid grains of soil, wetting fluid (i.e., pore water) and non-wetting fluid (i.e., pore air) [28,30]. The total soil strain change (ε_T) due to the effects of extrinsic factors is modelled as [33]

$$\varepsilon_T = \varepsilon_{es} + \varepsilon_{ms}, \tag{A1}$$

where ε_{es} is the volumetric strain driven by soil effective stress and ε_{ms} is the volumetric strain dependent on the saturation-moisture swelling relationship.

The behaviour of a mechanically-stabilised reactive soil mass that underwent a series of shrink–swell cycles is determined using

$$\sigma = \sigma' - S\psi_w. \tag{A2}$$

where σ is the total stress due to mechanical loads applied, σ' is the effective stress, ψ_w is the pore water pressure and S is the degree of saturation of the soil.

The resulting incremental coupled hydromechanical constitutive stress–strain law was taken as specified in Equation (4).

The shear behaviour of the soil was defined by specifying the Poisson's ratio, ν_{soil}. The instantaneous shear modulus, G, is then obtained using

$$G = \frac{E}{2(1+\nu_{soil})}, \tag{A3}$$

The deviatoric stress, σ_{dev}, is then written as

$$d\sigma_{dev} = Gd\varepsilon_{es}. \tag{A4}$$

Equation (A4) is integrated to obtain the total shear stress and total elastic shear strain relationship.

The calculation of ε_{ms} requires the moisture diffusion equation, sorption model and moisture swelling model. The three-dimensional water flow in variably saturated soil is described as

$$k_u\psi_w\left[\frac{\partial}{\partial x}\left(\frac{\partial h}{\partial x}\right)+\frac{\partial}{\partial y}\left(\frac{\partial h}{\partial y}\right)+\frac{\partial}{\partial z}\left(\frac{\partial h}{\partial z}\right)\right] = m_{sw}\gamma_w\frac{\partial h}{\partial t}, \tag{A5}$$

where k_u is the unsaturated soil permeability, h is the water potential head, m_{sw} is the slope of the soil–water characteristic curve (SWCC), γ_w is the unit weight of water and t is time.

The formulation of the unsaturated permeability is based on Forchheimer Law, which reads

$$k_u = f_{k_u} k_{sat} = \left(\frac{Q\gamma_w}{\partial(\psi_w)/\partial(L')} \right), \tag{A6}$$

where f_{k_u} is a factor of permeability dependent on saturation, k_{sat} is the permeability of fully saturated soils, Q is the volumetric water flux per unit area of soil, $\partial(\psi_w)/\partial(L')$ is the change in soil suction per unit length depending on the orthogonal axis being considered and ρ_w is the density of water. The factor, f_{k_u}, can be calculated as

$$f_{k_u} = S^3. \tag{A7}$$

The sorption model is described by a soil–water characteristic curve, SWCC, which defines the S-ψ_w relationship within the soil matrix using

$$\theta(\psi_w g^{-1}) = \theta_r + \frac{\theta_s - \theta_r}{(1 + |\alpha_{sw}\psi_w g^{-1}|^n)^m}, \tag{A8}$$

where $\theta(\psi_w g^{-1})$ is the volumetric soil moisture content, θ_r is the residual volumetric soil moisture content, θ_s is the volumetric soil moisture content at saturation, α_{sw}, n ($n > 1$) and m are empirical parameters reflecting the SWCC, with m calculated as

$$m = 1 - \frac{1}{n}. \tag{A9}$$

The weight and volume relationship of a soil can be used to transform θ to S, given by

$$S = \frac{\theta\rho_w G_s}{e\rho_b} = \frac{\omega G_s}{e}, \tag{A10}$$

where G_s is the specific gravity of solids of the soil, e is the void ratio and ρ_b is the bulk density of the soil. Using Equations (A5), (A6), (A8) and (A10), the time-dependent ε_{ms} can then be determined using the moisture swelling model presented in Figure A1b dependent to the corresponding S.

Under uniaxial loading, the stress–strain response remains linear elastic until the values of the failure stresses have attained the tension failure stress (σ_{t0}) and compression failure stress (σ_{c0}). Beyond the tension failure stress, σ_{t0}, micro-cracking appears represented macroscopically through softening response from the stress–strain curves. This leads to strain localization in the concrete. When the compression failure stress has been reached, in between σ_{c0} and the ultimate compression stress (σ_{cu}), the response is depicted by hardening of the stress–strain curves. Past σ_{cu}, softening of the stress–strain curves can be observed. CDP model assumes that curves can be converted into stress versus plastic-strain curves presented as

$$\sigma_t = \sigma_t(\tilde{\varepsilon}_t^{pl}, \dot{\tilde{\varepsilon}}_t^{pl}, T_m, f_i), \tag{A11}$$

$$\sigma_c = \sigma_c(\tilde{\varepsilon}_c^{pl}, \dot{\tilde{\varepsilon}}_c^{pl}, T_m, f_i), \tag{A12}$$

where $\tilde{\varepsilon}_t^{pl}$ and $\tilde{\varepsilon}_c^{pl}$ are the equivalent plastic strains, $\dot{\tilde{\varepsilon}}_t^{pl}$ and $\dot{\tilde{\varepsilon}}_c^{pl}$ are the equivalent plastic strain rates, T_m is the temperature of the concrete, and f_i are other variables being considered.

Deterioration of concrete occurs when unloading from any point on the strain softening plastic regime is performed. The elastic stiffness (E_0) is reduced due to the damage and weakening of the concrete, which is characterised by damage variables d_t and d_c for uniaxial tension and compression described as

$$d_t = d_t(\tilde{\varepsilon}_t^{pl}, T_m, f_i), \tag{A13}$$

$$d_c = d_c(\tilde{\varepsilon}_c^{pl}, T_m, f_i), \tag{A14}$$

where the values of d_t and d_c ranges from nil for undamaged concrete to one for concrete with total loss of strength. The stress–strain relationship under uniaxial tension and compression loading can be calculated as

$$\sigma_t = (1 - d_t)E_0(\varepsilon_t - \varepsilon_t^{pl}), \tag{A15}$$

$$\sigma_c = (1 - d_c)E_0(\varepsilon_c - \varepsilon_c^{pl}). \tag{A16}$$

Further details of CDP model are discussed in Dassault Systèmes [33].

Contact element analysis was applied to model the soil–structure interaction of reactive soils and raft footings. This methodology determines if the contact between the soil and the substructure are intact or separated with respect to support configuration, friction and penetration due to the interaction. Further details of the mechanics of contact elements are presented in Dassault Systèmes [33].

Appendix A.2. Numerical Simulations

The system of equations of the developed coupled hydromechanical model was solved by employing Abaqus CAE - SIMULIA^{TM} (Ver. 2017; https://www.3ds.com/ accessed on 24 July 2018). Numerical simulations were performed to compare the global performance of the developed prefabricated footing systems to monolithic waffle rafts for each site classification (i.e., Class M-D, H_1-D and H_2-D). The main objective is to investigate the deformation of footing systems due to the induced shrinking and swelling reactive soils and to compare the caused damage through soil–structure interaction. The validation of the developed model is summarised in the following sections. Furthermore, the details of the numerical simulations for the developed prefabricated footings and the monolithic waffle rafts are presented in the succeeding paragraphs.

Appendix A.2.1. Validation of the Developed Model

The developed hydromechanical finite element model [18,27] was used to investigate the global performance of the developed prefabricated footing systems. The developed model by [18,27] was validated using three case studies. The first case study verified the field data collected by Fityus et al. [53] in New Castle, Australia. The simulated ground movement and footing deformation were comparable to the monitored data in the field. The second case study validated the field data by [14] from Adelaide, Australia. The simulated soil–structure interaction and the damage experienced by a stiffened raft were similar to the site inspection and simulation in [14]. The third case study compared the developed coupled hydromechanical model to an uncoupled approach by [54]. The comparison highlighted the capability of the developed model to capture complex mound profiles that cannot be obtained using traditional uncoupled methods [18]. Moreover, mesh convergence and boundary effects studies were performed to determine the appropriate mesh size and required dimensions of the soil mass to prevent influence on the calculated soil movement values [27]. The recommended mesh size of the soil mass was 0.8 m. The applicable dimensions of the soil mass were 30 m for the width, more than three and a half times the length of the raft footing, and 12.5 m for the depth of the soil mass, which was at least eight times the depth of the raft footing.

Appendix A.2.2. Developed Prefabricated Footings and Monolithic Waffle Rafts

The reactive soil and the footing systems (i.e., the hypothetical developed prefabricated footings and the hypothetical monolithic waffle rafts) were symmetrical in x-axis and z-axis. Hence, only a quarter of the entire system was considered to save computational time. The quarter of the soil mass was 30 m by 30 m with a depth of 12.5 m. This was discretised using

a 0.8 m mesh size with a hexagonal structure and a linear pore fluid elements. The active depth zone, H_s, was assumed to be 3 m below the ground for all simulations. Important hydromechanical material properties of the reactive soil are presented in Figure A1. These properties are the soil–water characteristic curve or SWCC (Figure A1a) and the idealised moisture-swelling curve based on [38] (Figure A1b).

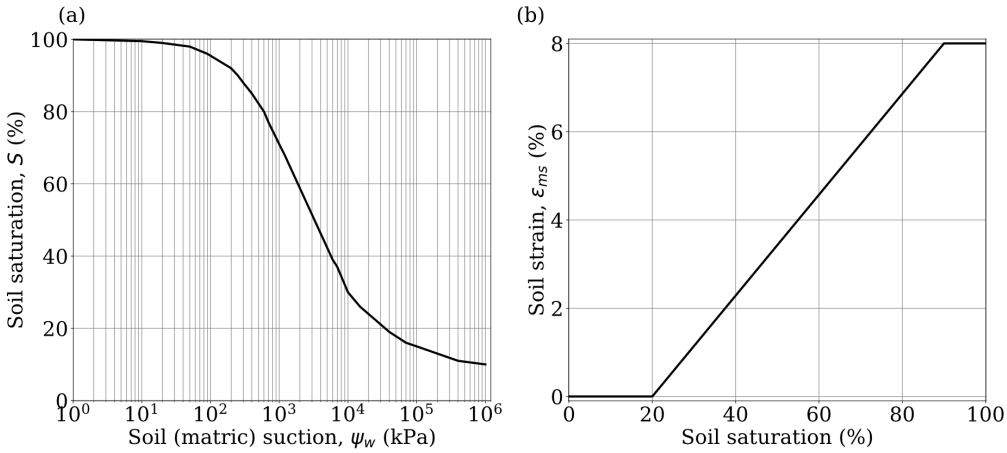

Figure A1. Input material properties of the reactive soil showing (**a**) the soil–water characteristic curve or SWCC from [18] and (**b**) the idealised moisture-swelling curve based on [38].

The footing systems were subjected to both swelling and shrinking movements of the reactive soil. The initial condition of the swelling and shrinking soil was assumed to have reached a stable state through equilibrium. Due to this assumption, the initial condition for each necessary parameters was uniformly specified throughout the soil mass. Considering the common initial condition in most sites, the initial swelling soil was assumed to have an initial value of u equal to -1.0×10^4 kPa [55]. Using the SWCC in Figure A1a, the corresponding value of S was 30%. The initial total stress, σ, was then calculated to be the product of the initial u and the initial S equivalent to -3.0×10^3 kPa. The initial void ratio (e) was assumed to be 1.2 for both swelling and shrinking soils. The initial condition of shrinking soil was assumed to have an initial value of u equal to -6.0×10^2 kPa, corresponding to a value of S equal to 80%. The initial σ was calculated to be equal to -4.8×10^2 kPa. The numerical analyses considered two steps, the first step was a geostatic analysis conducted to set-up the in-situ stresses and to cancel out soil deformation due to the initial condition. The second step used a transient flow-deformation analysis where the final value for each swelling and shrinking scenario was specified on the uncovered ground surface exposed to precipitation and evapotranspiration. The final value of u at the uncovered ground was determined by considering the average change in soil suction, $\Delta\overline{u}$, stipulated in [24] equal to 1.2 pF. Hence, considering the initial values of u and the value of $\Delta\overline{u}$, values of the final u were -6.0×10^2 kPa and -1×10^4 kPa for swelling and shrinking soils, respectively. Simulations were then terminated when a change in u below the assumed active depth zone, H_s = 3 m, had eventuated.

Boundary conditions of the outer surfaces of the soil mass were restrained horizontally with vertical movements unrestrained. The inner surfaces of both the soil mass and the footing systems were x-symmetry and z-symmetry since only a quarter of the entire system was simulated.

The soil–structure interaction between the swelling-shrinking reactive soil and the hypothetical footing systems was defined by a friction contact using a penalty friction coefficient, μ_{sc}, of 0.35 allowing separation [38]. The concrete-concrete interaction of the developed prefabricated footing systems was defined using a penalty friction coefficient, μ_{cc}, equal to 0.40 based on the common value used for prefabricated construction and allowing separation.

The developed prefabricated footing systems and the monolithic waffle rafts were assumed to have a constant floor area of 225 m^2 (15 by 15 m^2) based on the average floor area of single-detached dwellings [18]. The elastic modulus of concrete, E_c, was taken as 27 GPa with a Poisson's ratio, ν_c, of 0.2. The density of concrete was 2400 kg m^{-3}. The slab thickness of the prefabricated raft footing system was 125 mm, while that of the waffle raft was 85 mm. The developed prefabricated footing required a thicker deck slab since performed structural analyses attained excessive slab deflection when the slab thickness was thinner than 125 mm. A factored area load (p) equal to 2.5 kN m^{-2} and a factored line load (q) equal to 6.5 kN m^{-1} were applied onto the slab and the edges of the footing systems, assuming that the superstructure construction is an articulated masonry veneer for all simulations. The CDP model was employed for the concrete material property, considering the non-linear plastic material behaviour, described in Figure A2.

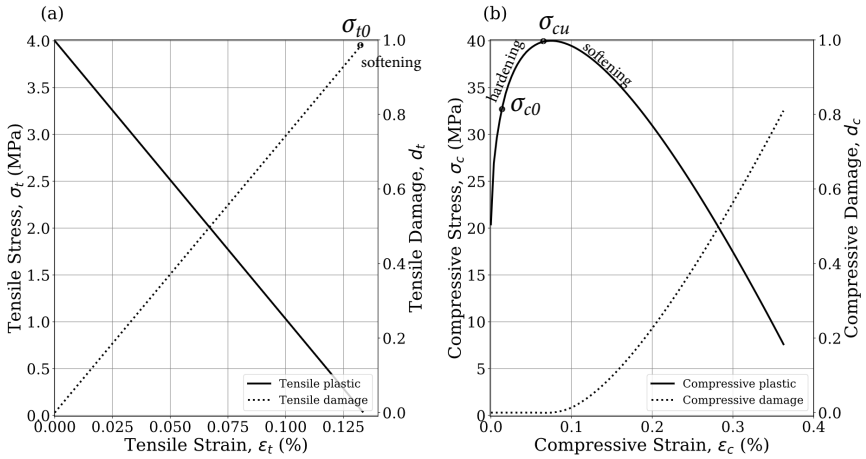

Figure A2. Input material properties for the Concrete Damaged Plasticity (CDP) model. The response of the CDP model for (**a**) uniaxial tensile loading and (**b**) uniaxial compressive loading are presented.

Appendix B. Supplementary Results of the Numerical Simulations

Damage to footing systems was induced by the shrink–swell ground movement through soil–structure interaction. The absence of soil contact with the footing system when edge heave and centre heave takes place caused the substructures to behave as simply-supported or cantilevered elements (Figure 1). A value of cracking damage d_t or DAMAGET > 0 reflects concrete cracking. These are classified as hairline cracks when $d_t < 0.25$, fine but noticeable cracks when $0.25 \leq d_t < 0.85$, distinct cracks when $0.85 \leq d_t < 0.99$, and wide cracks or gaps when $d_t \geq 0.99$ [24].

In the edge heave scenario where the uncovered soil swelled, the experienced cracking damage (d_t or DAMAGET) of the developed prefabricated footings and the monolithic waffle rafts are shown in Figure A3. It can be observed that the cracking damage, d_t, for Site Classes M/M-D and H_1/H_1-D fine cracks yet noticeable at the bottom portion of the footing systems. The cracking damage under the developed prefabricated footing systems for Site Classes M-D and H_1-D was around the edge beams and at the 4-way connector (Figure A3a,c). On the other hand, the monolithic waffle rafts for Site Classes M/M-D and H_1/H_1-D were around the third to fourth internal beams (Figure A3b,d). For Site Class H_2-D, both cracking damage occurred in the developed prefabricated footing and monolithic waffle raft ranged from hairline cracks to wide cracks or gaps considered as structural damage (Figure A3e,f). The prefabricated system mostly experienced the structural damage in the DEB element, which is desirable since the connection was transferring the forces and moments effectively. The monolithic waffle raft experienced most structural damage close to the centre of the entire footing system, which is logical since the centre is the critical area for suspended structural elements. Figure A4 shows the yielding of steel. It can be observed that the yielding of steel in the prefabricated systems and the monolithic waffle rafts were in a similar area where the simulated cracking propagated.

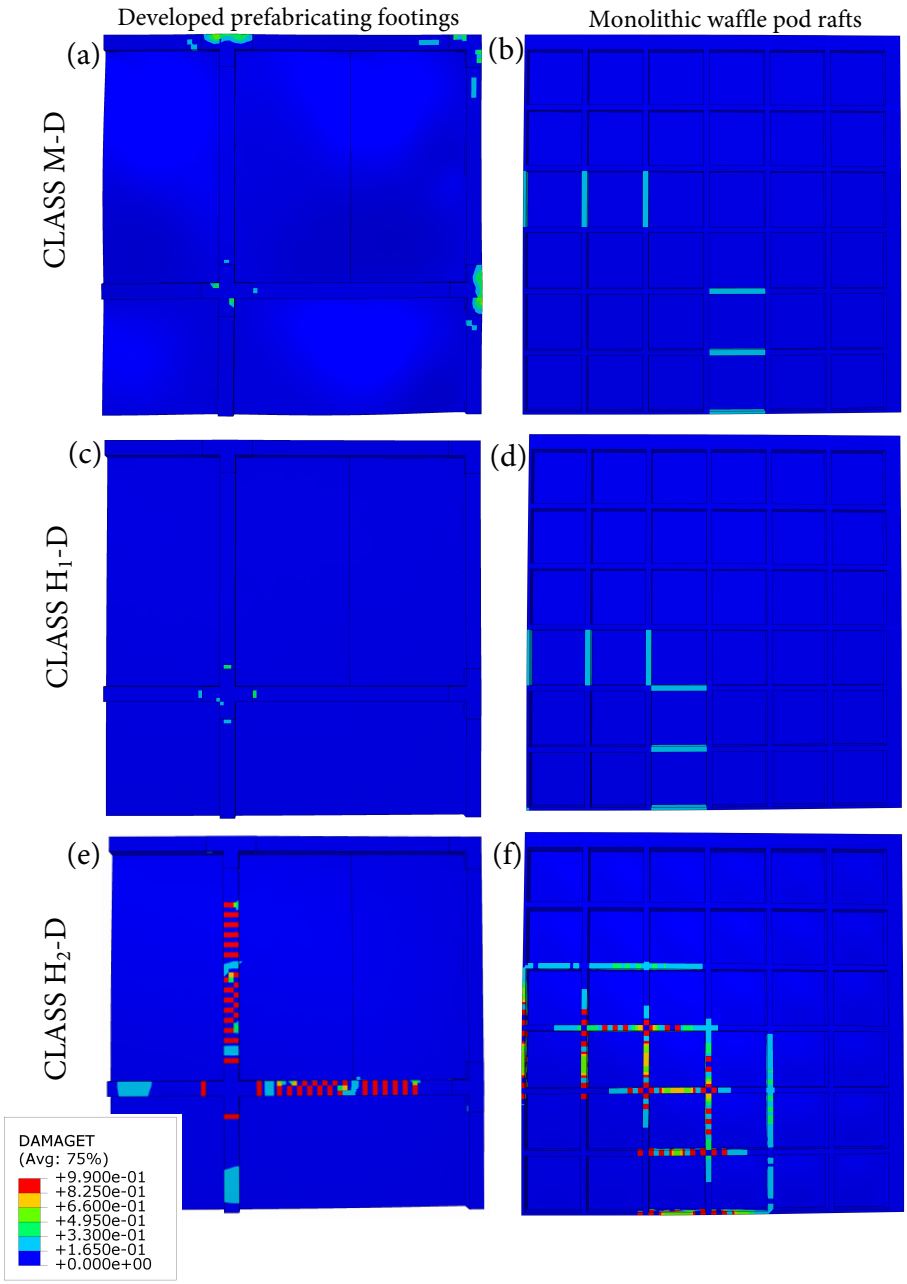

Figure A3. Comparison of footing damage due to swelling soil between the developed prefabricated footing systems and waffle rafts for (**a**,**b**) Class M-D soil, (**c**,**d**) Class H_1-D soil, and (**e**,**f**) Class H_2-D soil. A value of DAMAGET (d_t) greater than zero reflects concrete cracking, classified as: DAMAGET (d_t) < 0.25 = hairline cracks, $0.25 \leq$ DAMAGET (d_t) < 0.85 = fine but noticeable cracks, $0.85 \leq$ DAMAGET (d_t) < 0.99 = distinct cracks, and DAMAGET (d_t) ≥ 0.99 = wide cracks or gaps [24].

In the centre heave scenario where the uncovered soil shrank, the d_t or DAMAGET of the developed prefabricated footings and the monolithic waffle rafts are shown in Figure A5. The developed prefabricated footing for Site Class M-D experienced minor structural damage at the three-way connectors (Figure A5a). Contrarily, the monolithic waffle raft for Site Class M-D experienced extensive linear structural damage that started from the re-entrant corner and propagated through the beam and slabs (Figure A5b). The developed prefabricated footing systems for Classes H_1/H_1-D and H_2/H_2-D had localised structural damage around the bolt connections (Figure A5c,e). This indicates that when the line loads were applied onto the prefabricated footing systems acting as a cantilever, the bolt connection and steel reinforcements moved outwardly and yielded due to the negative

moment experienced by the systems. Thus, the governing failure was around the bolt connections keeping the whole prefabricated systems intact and jointed. To mitigate this, a perimeter piling can be installed. On the other hand, extensive structural damage was observed in the monolithic waffle rafts for Classes H_1-D and H_2-D (Figure A5d,f). Severe structural damage was experienced close to the perimeter, which was around the second to third internal beams from the edge beams. This was due to the lack of reinforcements to resist the negative moment, which only relied on the mesh of the slab.

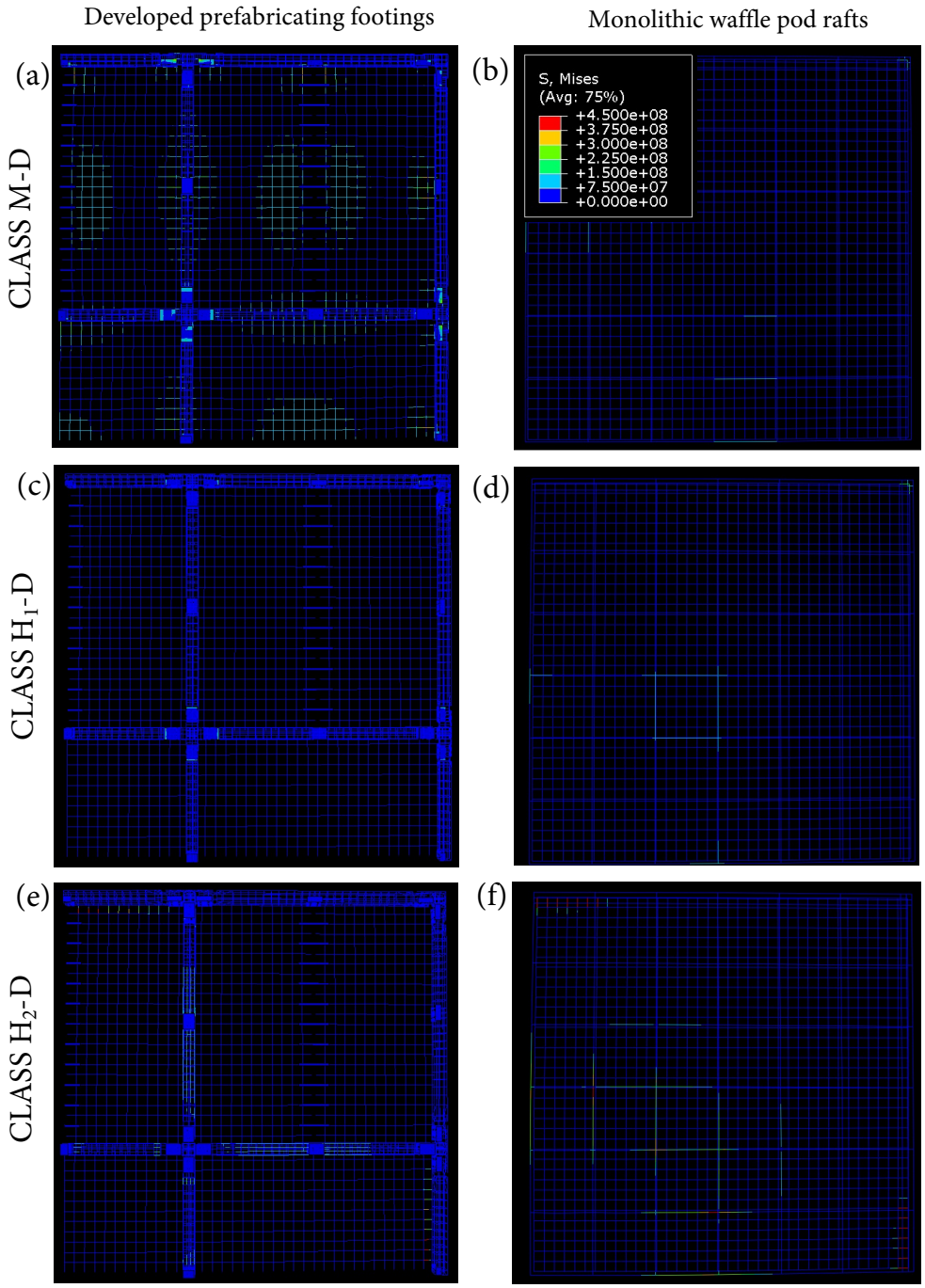

Figure A4. Comparison of steel stress in footing systems due to swelling soil and applied loads between the developed prefabricated footing systems and waffle rafts for (**a**,**b**) Class M-D soil, (**c**,**d**) Class H_1-D soil, and (**e**,**f**) Class H_2-D soil. Values of stress are in Pascal.

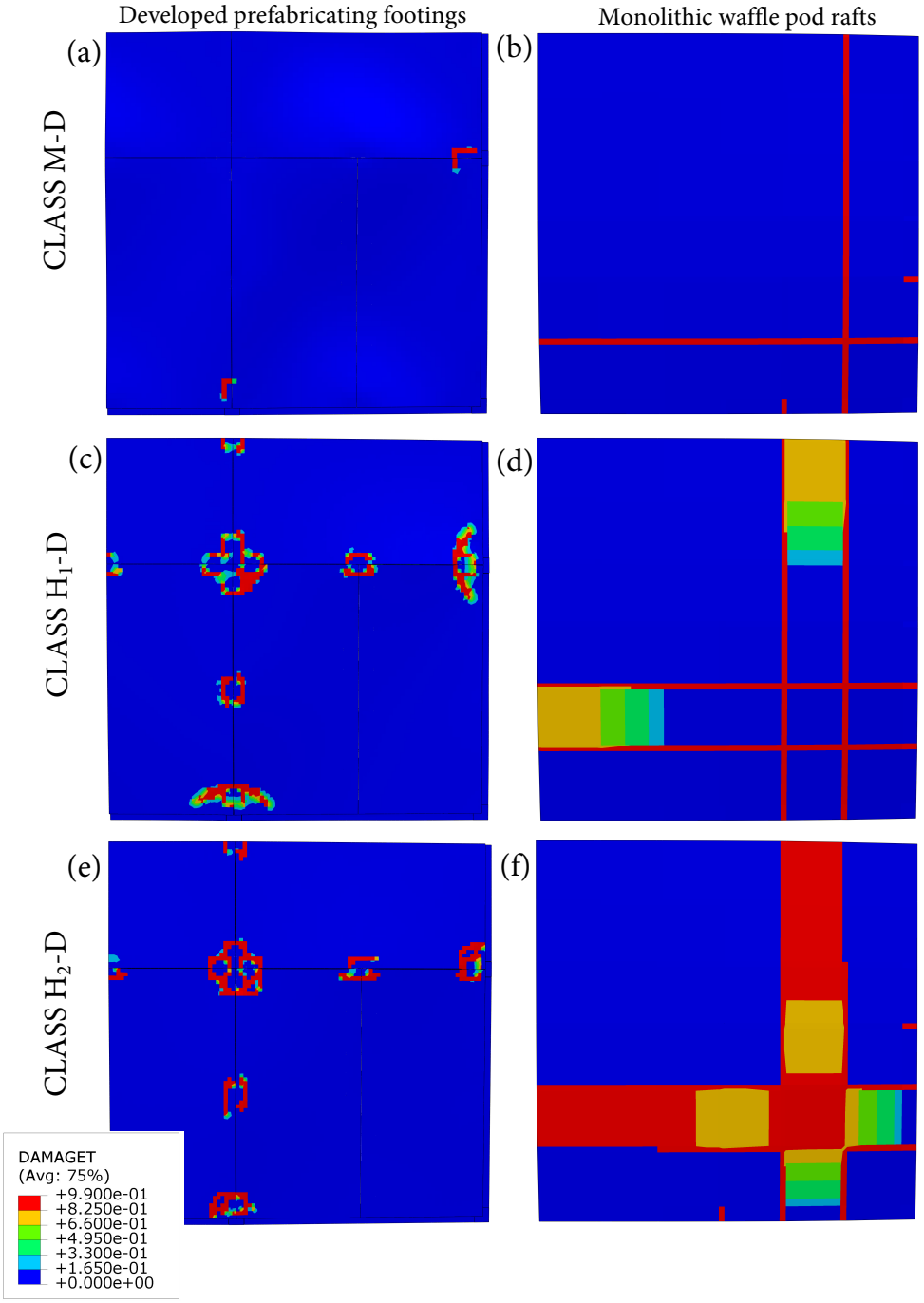

Figure A5. Comparison of footing damage due to shrinking soil between the developed prefabricated footing systems and waffle rafts for (**a**,**b**) Class M-D soil, (**c**,**d**) Class H_1-D soil, and (**e**,**f**) Class H_2-D soil. A value of DAMAGET (d_t) greater than zero reflects concrete cracking, classified as: DAMAGET (d_t) < 0.25 = hairline cracks, $0.25 \leq$ DAMAGET (d_t) < 0.85 = fine but noticeable cracks, $0.85 \leq$ DAMAGET (d_t) < 0.99 = distinct cracks, and DAMAGET (d_t) ≥ 0.99 = wide cracks or gaps [24].

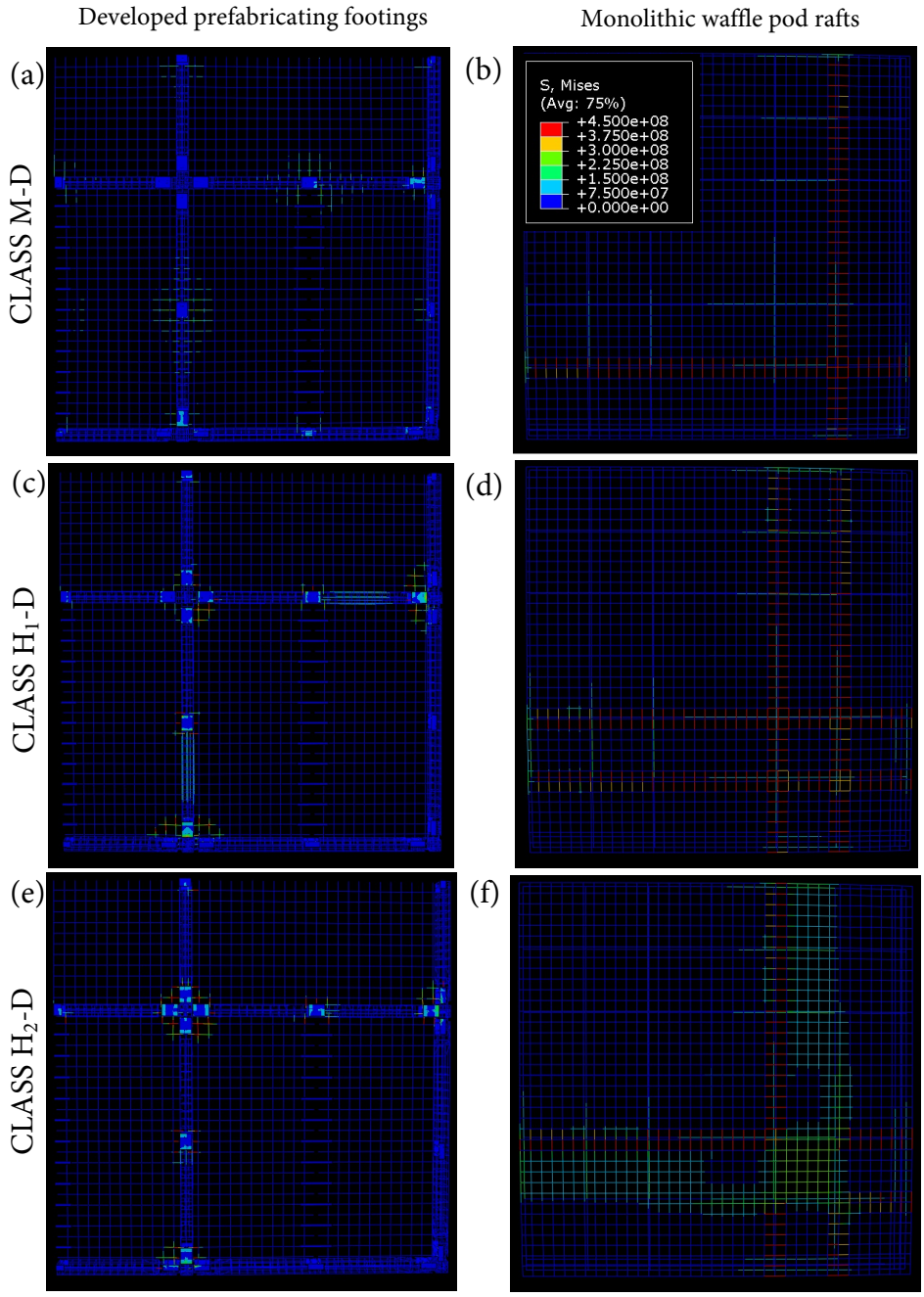

Figure A6. Comparison of steel stress in footing systems due to shrinking soil and applied loads between the developed prefabricated footing systems and waffle rafts for (**a**,**b**) Class M-D soil, (**c**,**d**) Class H_1-D soil, and (**e**,**f**) Class H_2-D soil. Values of stress are in Pascal.

References

1. Azman, M.; Ahamad, M.; Hussin, W. Comparative study on prefabrication construction process. *Int. Surv. Res. J.* **2012**, *2*, 45–58.
2. Lichtenberg, J. Slimbouwen, a strategy for efficient and sustainable building innovation. In *Construction in the XXI Century: Local and global challenges, Symposium Proceedings, CIB W065/N055/W086, Rome, Italy, October 2006*; pp. 206–207. Available online: http://hdl.handle.net/1822/6794 (accessed on 10 October 2021).
3. Ross, K.; Cartwright, P.; Novakovic, O. *A Guide to Modern Methods of Construction*; IHS BRE Press: London, UK, 2006.
4. Wong, R.; Hao, J.; Zou, P. The application of precast concrete technology in buildings and civil structures construction: Hong Kong experience. In Proceedings of the Second International Conference on Construction in the 21st Century (CITC-II), Sustainability and Innovation in Management and Technology, Hong Kong, China, 10–12 December 2003; pp. 629–634.

5. Gibb, A.G. *Off-Site Fabrication: Prefabrication, Pre-Assembly and Modularisation*; John Wiley & Sons: Hoboken, NJ, USA, 1999.
6. Ngwepe, L.; Aigbavboa, C. A theoretical review of building life cycle stages and their related environmental impacts. *J. Civil Eng. Environ. Technol.* **2015**, *2*, 7–15.
7. Aye, L.; Ngo, T.; Crawford, R.H.; Gammampila, R.; Mendis, P. Life cycle greenhouse gas emissions and energy analysis of prefabricated reusable building modules. *Energy Build.* **2012**, *47*, 159–168.
8. Sharma, A.; Saxena, A.; Sethi, M.; Shree, V.; Varun. Life cycle assessment of buildings: A review. *Renew. Sustain. Energy Rev.* **2011**, *15*, 871–875.
9. Piroozfar, A.E.; Larsen, O.P.; Altan, H. Customization in building design and construction: A contribution to sustainability. In *Handbook of Research in Mass Customization and Personalization: (In 2 Volumes)*; World Scientific: Singapore, 2010; pp. 911–939.
10. Smith, D.; Tardif, M. *BIM: A Strategic Implementation Guide for Architects, Engineers, Constructors and Real Estate Asset Managers*; Wiley: Hoboken, NJ, USA, 2009.
11. Nelson, S. Modular housing: Prefab and proudly upmarket. *Build. Connect.* **2008**, 24.
12. Pujadas Gispert, E. Prefabricated Foundations for Housing Applied to Room Modules. Ph.D. Thesis, Universitat Politecnica de Catalunya, Barselona, Spain, 2016.
13. Teodosio, B.; Baduge, K.S.K.; Mendis, P.; Heath, D. Prefabrication of substructures for single-detached dwellings on reactive soils: A review of existing systems and design challenges. *Aust. J. Civ. Eng.* **2019**, *7*, 120–133. doi:10.1080/14488353.2019.1657056.
14. Li, J.; Cameron, D.A.; Ren, G. Case study and back analysis of a residential building damaged by expansive soils. *Comput. Geotech.* **2014**, *56*, 89–99.
15. Li, J. Analysis and Modelling of Performance of Footings on Expansive Soils. Ph.D. Thesis, 1996.
16. Teodosio, B.; Baduge, S.K.; Mendis, P.; Heath, D. Soil-structure interaction design methods for residential structures on reactive soils. In Australian Structural Engineering Conference: ASEC 2018; Engineers Australia: Barton, ACT, Australia, 2018; p. 49.
17. Teodosio, B.; Baduge, K.S.K.; Mendis, P. A review and comparison of design methods for raft substructures on expansive soils. *J. Build. Eng.* **2021**, *41*, 102737.
18. Teodosio, B.; Baduge, K.S.K.; Mendis, P. Simulating reactive soil and substructure interaction using a simplified hydro-mechanical finite element model dependent on soil saturation, suction and moisture-swelling relationship. *Comput. Geotech.* **2020**, *119*, 1–18.
19. Li, J.; Cameron, D.A. Case study of courtyard house damaged by expansive soils. *J. Perform. Constr. Facil.* **2002**, *16*, 169–175.
20. Jones, L.D.; Jefferson, I. Expansive soils. In *ICE Manual of Geotechnical Engineering*; ICE: London, UK, 2012; pp. 413–441.
21. Miao, L.; Wang, F.; Cui, Y.; Shi, S. Hydraulic characteristics, strength of cyclic wetting-drying and constitutive model of expansive soils. In Proceedings of the 4th International Conference on Problematic Soils, Wuhan, China, 21–23 September 2012; pp. 303–322.
22. Skinner, H.; Crilly, M.; Charles, J. Numerical Models for the Design of Shallow Foundations for Low-rise Buildings. In *Application of Numerical Methods to Geotechnical Problems*; Springer: Berlin, Germany, 1998; pp. 655–664.
23. Krohn, J.P.; Slosson, J.E.Y. Assessment of expansive soils with the United States.
24. Standards Australia. *AS 2870-2011: Residential Slabs and Footings*; Standards Australia: Sydney, Australia, 2011.
25. American Society for Testing and Materials. *Standard Guide for Dimensional Coordination of Rectilinear Building Parts and Systems*; American Society for Testing and Materials: West Conshohocken, PA, USA, 2002.
26. Bergvall, L. Dimensional Coordination as a Tool for Industrialisation. In *Metric Dimensional Coordination—The Issue and Precedent*; US Department of Commerce, National Bureau of Standards: Gaithersburg, MD, USA, 1977; pp. 203–204.
27. Teodosio, B.; Baduge, K.S.K.; Mendis, P. Relationship between reactive soil movement and footing deflection: A coupled hydro-mechanical finite element modeling perspective. *Comput. Geotech.* **2020**, *126*, 103720.
28. Kim, S.; Ahn, J.; Teodosio, B.; Shin, H. Numerical analysis of infiltration in permeable pavement system considering unsaturated characteristics. *J. Korean Soc. Disaster Inf.* **2015**, *11*, 318–328.
29. Teodosio, B.; Ahn, J.; Shin, H.S. Numerical analysis of infiltration into pervious concrete-base systems. *Int. J. GEOMATE Geotech. Constr. Mater. Environ.* **2015**, *8*, 1117–1122.
30. Weerasinghe, D. A Failure Analysis of Small-Diameter Cast Iron Pipes in Reactive Soil Zones of Melbourne. Ph.D. Thesis, Monash University, Clayton, Australia, 2018.
31. Rutqvist, J.; Börgesson, L.; Chijimatsu, M.; Kobayashi, A.; Jing, L.; Nguyen, T.; Noorishad, J.; Tsang, C.F. Thermohydromechanics of partially saturated geological media: governing equations and formulation of four finite element models. *Int. J. Rock Mech. Min. Sci.* **2001**, *38*, 105–127.
32. Hillerborg, A.; Modéer, M.; Petersson, P.E. Analysis of crack formation and crack growth in concrete by means of fracture mechanics and finite elements. *Cem. Concr. Res.* **1976**, *6*, 773–781.
33. Dassault Systèmes. Abaqus 6.14: Online Documentation Help, Theory Manual, 2016. Available online: http://130.149.89.49:2080/v6.14/ (accessed on 24 July 2018).
34. Standards Australia. *AS 1289.3. 6.1 2009: Standard Method of Analysis by Sieving in Methods of Testing Soils for Engineering Purposes*; SAI Global: Brisbane, Australia, 2009.
35. Schofield, A.; Wroth, P. *Critical State Soil Mechanics*; McGraw-Hill: London, UK, 1968; Volume 310.
36. Altmann, J.B.; Müller, T.M.; Müller, B.I.; Tingay, M.R.; Heidbach, O. Poroelastic contribution to the reservoir stress path. *Int. J. Rock Mech. Min. Sci.* **2010**, *47*, 1104–1113.
37. Altmann, J. Poroelastic Effects in Reservoir Modeling. Ph.D. Thesis, Universität Karlsruhe, Karlsruhe, Germany, 2010.

38. Shams, M.A.; Shahin, M.A.; Ismail, M.A. Simulating the behaviour of reactive soils and slab foundations using hydro-mechanical finite element modelling incorporating soil suction and moisture changes. *Comput. Geotech.* **2018**, *98*, 17–34.
39. Schaap, M.G.; Leij, F.J.; Van Genuchten, M.T. Rosetta: A computer program for estimating soil hydraulic parameters with hierarchical pedotransfer functions. *J. Hydrol.* **2001**, *251*, 163–176.
40. Standards Australia. *AS 1170.1-1989, Part 1: Dead and Live Loads and Load Combinations*; SAI Global: Brisbane, Austrlia, 1989.
41. Briaud, J.L.; Abdelmalak, R.; Zhang, X.; Magbo, C. Stiffened Slab-On-Grade on Shrink-Swell Soil: New Design Method. *J. Geotech. Geoenviron. Eng.* **2016**, *142*, 04016017.
42. Potyondy, J.G. Skin friction between various soils and construction materials. *Geotechnique* **1961**, *11*, 339–353.
43. Standards Australia. *AS 3600–2009: Concrete Structures*; SAI Global: Brisbane, Australia, 2009.
44. ISO. *Buildings and Constructed Assets-Service-Life Planning. 5. Life-Cycle Costing*; ISO: Geneva, Switzerland, 2008.
45. Asamoah, R.O.; Ankrah, J.S.; Offei-Nyako, K.; Tutu, E.O. Cost analysis of precast and cast-in-place concrete construction for selected public buildings in Ghana. *J. Constr. Eng.* **2016**, *2016*, 8785129.
46. Chan, T.K. Comparison of precast construction costs—Case studies in Australia and Malaysia. In Proceedings of the 27th Annual ARCOM Conference, Bristol, UK, 5–7 September 2011; pp. 3–12.
47. Rawlinsons. *Rawlinsons Construction Cost Guide 2019*; Rawlinsons: Rivervale, Australia, 2019.
48. De Normalisation, C.E. *EN 15978 Sustainability of Construction Works—Assessment of Environmental Performance of Buildings–Calculation Method*; CEN: Brussels, Belgium, 2012.
49. Crawford, R.H.; Stephan, A.; Prideaux, F. *Environmental Performance in Construction (EPiC) Database*; 2019. Available online: https://melbourne.figshare.com/articles/book/EPiC_Database/10257728 (accessed on 10 October 2021).
50. AusLCI. *Australian Life Cycle Inventory Database, Australian Life Cycle Assessment Society (ALCAS)*; 2017.
51. Hong, T.; Ji, C.; Jang, M.; Park, H. Assessment model for energy consumption and greenhouse gas emissions during building construction. *J. Manag. Eng.* **2014**, *30*, 226–235.
52. Ahmed, I.M.; Tsavdaridis, K.D. Life cycle assessment (LCA) and cost (LCC) studies of lightweight composite flooring systems. *J. Build. Eng.* **2018**, *20*, 624–633.
53. Fityus, S.; Smith, D.; Allman, M. Expansive soil test site near Newcastle. *J. Geotech. Geoenviron. Eng.* **2004**, *130*, 686–695.
54. Mitchell, P. A simple method of design of shallow footings on expansive soil. In Proceedings of the Fifth International Conference on Expansive Soils 1984: Preprints of Papers, Institution of Engineers, Adelaide, SA, Australia, 21–23 May 1984; p. 159.
55. Zou, J. *Assessment of the Reactivity of Expansive Soil in Melbourne Metropolitan Area*; Royal Melbourne Institute of Technology: Melbourne, Australia, 2015.